Characterization of an Australian outbreak Japanese Encephalitis virus genotype 4 isolate in mice and human cortical brain organoids

Wilson Nguyen[a], Romal Stewart[a], Bing Tang[a], Kexin Yan[a], Thibaut Larcher[b], Cameron Bishop[a], Narayan Gyawali[a], Gregor Devine[a], Andreas Suhrbier[a,c], Daniel J. Rawle[a*].

[a] QIMR Berghofer Medical Research Institute, Brisbane, Queensland 4029, Australia.
[b] INRAE, Oniris, PAnTher, APEX, Nantes, France.
[c] GVN Center of Excellence, Australian Infectious Disease Research Centre, Brisbane, Queensland, 4029 and 4072, Australia.

[*]Corresponding author. Email: Daniel.Rawle@qimrberghofer.edu.au

A.S. D.J.R. joint last.

ABSTRACT

Human infections with Japanese encephalitis virus (JEV) are a leading cause of viral encephalitis, with ≈70,000 symptomatic cases (≈40% with long-term neurological sequelae) and ≈20,000 deaths reported annually, primarily in Asia and the Western Pacific. An outbreak of JEV genotype 4 was also recently reported in Australia, with an isolate ($JEV_{NSW/22}$) obtained from a stillborn piglet. Herein we characterize the neuropathology of $JEV_{NSW/22}$, JEV_{FU} (genotype 2) and $JEV_{Nakayama}$ (genotype 3) in adult C57BL/6J wild-type mice, mice deficient in interferon regulatory factor 7 ($IRF7^{-/-}$), and mice deficient in the type I interferon receptor ($IFNAR^{-/-}$). In C57BL/6J and $IRF7^{-/-}$ mice with lethal outcomes, viral antigen was detected by immunohistochemistry in *inter alia* the cortex, thalamus and hippocampus. In these mice, histological lesions included neuronal degeneration, neuronal vacuolation, perivascular cuffing, leukocyte infiltrates, hemorrhage, and microgliosis, with apoptosis and astrocyte activation detected by immunohistochemistry. Microgliosis and hemorrhage persisted in some surviving mice ≈3-4 weeks post infection. JEV was universally lethal in $IFNAR^{-/-}$ mice by day 3 with histological signs of brain hemorrhage, but produced no other detectable brain infection or lesions, with NS1 readily detected in blood vessels, but not neurons, by immunohistochemistry. All JEV isolates showed robust productive cytopathic infection of human cortical brain organoids (hBOs), as well as a human neural progenitor cell line (RENcell VM). We thus describe a new $IRF7^{-/-}$mouse model for JEV, which shows increased penetrance of lethal neuroinvasiveness and recapitulates many aspects human disease. Although less virulent in $IRF7^{-/-}$ mice, $JEV_{NSW/22}$ retained the capacity to cause lethal encephalitis and to replicate and destroy human neuronal cells.

Introduction

Japanese Encephalitis virus (JEV) is a single-stranded positive-sense RNA virus from the *Flaviviridae* family that is transmitted from amplifying hosts (primarily pigs and wading birds) via mosquitoes to humans [1]. While infection is usually asymptomatic, encephalitis can develop in ≈1 in 250 people, with ~30% of encephalitic cases becoming fatal, and 30-50% of non-fatal encephalitic cases retaining persistent neurological symptoms including seizures, speech impediments and paralysis [2,3]. JEV is the leading cause of viral encephalitis in Asia, with ~70,000 cases and ~20,000 deaths per annum [4]. After a bite from an infected mosquito, JEV replicates in peripheral blood monocytes producing a viremia that, in some cases, leads to virus crossing the blood brain barrier [5]. JEV primarily infects neurons in the brain [6] leading to uncontrolled inflammation (encephalitis) and neuronal cell death [2]. There are several available and effective vaccines against JEV [7], but there are no specific licensed treatments.

Efforts to develop treatments for JEV neuropathology are hindered by the difficulties in diagnosing early infection [8] before the virus has infected central nervous system (CNS) neurons; and once the virus has infected CNS neurons, treatments must also be able to effectively enter the brain. In addition, mouse models of JEV neuropathology are often physiologically inappropriate, using intracranial routes of infection or very young mice [9-11]. Well-characterized, adult mouse models with high penetrance of JEV neuropathology after peripheral inoculation would represent useful tools to study mechanisms of infection and disease and evaluate potential new interventions.

JEV exists as five genotypes (G1-G5) which are phylogenetically, antigenically and geographically distinct [12-14]. G3 was the main genotype endemic in Asia until 1990, after which genotype I has dominated since [15]. G2 has been identified in Malaysia, Indonesia, Papua New Guinea and Australian outbreaks from 1970-2000. G5 has been identified in China, and is now dominant in South Korea [16]. G4 was the least common genotype worldwide, having only been identified in mosquitoes from Indonesia and Papua New Guinea [8]. In February 2021, a fatal JEV infection occurred on the Tiwi Islands, 80 km off the coast of Darwin, Australia [17]. Sequencing identified that the virus belonged to the rare JEV G4 [17]. In 2022, a geographically widespread outbreak throughout most Australian states was attributed to JEV G4, which caused 44 confirmed human cases and 7 deaths [18]. Outbreaks occurred in several piggeries, causing high abortion and stillbirth rates in sows [19]. Based on proximity to piggeries, estimates indicate that

~740,000 people may be at risk of being infected by JEV in Australia [19]. Given that *Culex annulirostris* mosquitoes, considered the primary vector for JEV in Australia [18,19], and amplifying vertebrate hosts including wading birds and pigs are widespread, it is possible that JEV may become, or is already, endemic in Australia [18]. Murray Valley Encephalitis virus (MVEV) and Kunjin virus are phylogenetically closely related to JEV and have similar vector and reservoir hosts, and are endemic to Australia [20].

Herein, we characterize a new JEV mouse model using IRF7$^{-/-}$ mice, which shows high penetrance of CNS infections, as well as neuropathology that recapitulates many aspects seen in human post mortem brain specimens. We also describe for the first time the behavior of a recent JEV G4 isolate from the Australian outbreak in mice and in human cortical brain organoids.

Materials and methods

Ethics statement and regulatory compliance

All mouse work was conducted in accordance with the "Australian code for the care and use of animals for scientific purposes" as defined by the National Health and Medical Research Council of Australia. Mouse work was approved by the QIMR Berghofer Medical Research Institute Animal Ethics Committee (P3746, A2108-612). Mice were euthanized using CO_2 or cervical dislocation.

Breeding and use of GM mice was approved under a Notifiable Low Risk Dealing (NLRD) Identifier: NLRD_Suhrbier_Oct2020: NLRD 1.1(a). Use of Imojev was approved under NLRD_Suhrbier_Oct2019: NLRD2.1(d).

All infectious JEV work was conducted in a dedicated suite in a biosafety level-3 (PC3) facility at the QIMR Berghofer MRI (Australian Department of Agriculture, Water and the Environment certification Q2326 and Office of the Gene Technology Regulator certification 3445). All work was approved by the QIMR Berghofer Medical Research Institute Safety Committee (P3746).

Cell lines and culture

Vero E6 (C1008, ECACC, Wiltshire, England; obtained via Sigma Aldrich, St. Louis, MO, USA) and C6/36 cells (ATCC# CRL-1660) were cultured in medium comprising RPMI 1640 (Gibco), supplemented with 10% fetal bovine serum (FBS), penicillin (100 IU/ml)/streptomycin (100 μg/ml) (Gibco/Life Technologies) and L-glutamine (2 mM) (Life Technologies). Cells

were cultured at 37°C and 5% CO_2. Cells were routinely checked for mycoplasma (MycoAlert Mycoplasma Detection Kit MycoAlert, Lonza) and FBS was assayed for endotoxin contamination before purchase [21].

RENcell VM Human Neural Progenitor Cell Line (Sigma Aldrich) were cultured in medium comprising DMEM F-12 (Thermo Fisher Scientific), penicillin (100 IU/ml)/streptomycin (100 µg/ml) (Gibco/Life Technologies), 20 ng/ml FGF (STEMCELL Technologies), 20 ng/ml EGF (STEMCELL Technologies), and 2% B27 supplements (Thermo Fisher Scientific). Cells were detached using StemPro Accutase Cell Dissociation Reagent (Thermo Fisher Scientific), and were cultured in Matrigel (Sigma). For crystal violet staining of remaining cells after infection, formaldehyde (7.5% w/v)/crystal violet (0.05% w/v) was added to wells overnight, plates washed twice in water, and plates dried overnight.

Virus isolates and culture

$JEV_{Nakayama}$ (GenBank: EF571853), JEV_{FU} (GenBank: AF217620), and Imojev were a gift from Assoc. Prof. Gregor Devine (QIMR Berghofer MRI). $JEV_{NSW/22}$ (GenBank: OP904182) was a gift from Dr. Peter Kirkland (Elizabeth Macarthur Agriculture Institute, New South Wales, Australia). $MVEV_{TC123130}$ (GenBank: JN119814.1) was obtained from the "Doherty Virus Collection" currently held at QIMR Berghofer MRI. Virus stocks were generated by infection of C6/36 cells (for JEV and MVEV) or Vero E6 cells (for Imojev and YFV 17D) at multiplicity of infection (MOI) ≈0.1, with supernatant collected after ~5 days, cell debris removed by centrifugation at 3000 x g for 15 min at 4°C, and virus aliquoted and stored at -80°C. Virus titers were determined using standard $CCID_{50}$ assays (see below).

$CCID_{50}$ assays

Vero E6 cells were plated into 96 well flat bottom plates at $2x10^4$ cells per well in 100 µl of medium. For tissue titrations, tissues were homogenized in tubes each containing 4 ceramic beads twice at 6000 x g for 15 seconds, followed by centrifugation twice at 21,000 x g for 5 min before 5 fold serial dilutions in 100 µl RPMI 1640 supplemented with 2% FBS. For cell culture supernatant or mouse serum, 10 fold serial dilutions were performed in 100 µl RPMI 1640 supplemented with 2% FBS. A volume of 100 µl of serially diluted samples were added to each well of 96 well plate containing Vero E6 cells and the plates cultured for 5-7 days at 37°C and

5% CO_2. The virus titer was determined by the method of Spearman and Karber.

Mouse infections

C57BL/6J mice were purchased from the Animal Resources Center, Canning Vale WA, Australia. IFNAR$^{-/-}$ were kindly provided by Dr P. Hertzog (Monash University, Melbourne, Australia). IRF7$^{-/-}$ mice were kindly provided by T. Taniguchi (University of Tokyo) [22-24]. C57BL/6N mice were purchased from The Jackson Laboratory (stock no. 005304). C57BL/6NJ$^{\Delta Nnt8\text{-}12}$ were generated by The Australian Phenomics Network, Monash University, Melbourne, Australia as described [25]. Mice used in this study were female, except IRF7$^{-/-}$ mice where both males and females were used. The age/age range at infection is indicated in the figure legends. Mice were sorted into groups so that each group had a similar mean age and age distribution, and in the case of IRF7$^{-/-}$ mice, had equal numbers of males and females in each group. All mice strains except C57BL/6J were bred in-house at QIMR Berghofer MRI, and mice housing conditions were described previously [26]. Mice were infected subcutaneously (s.c.) at the base of the tail with 100 µl of virus inoculum. Serum was collected via tail nicks in to Microvette Serum-Gel 500 µl blood collection tubes (Sarstedt, Numbrecht, Germany). Mice were weighed and monitored for disease manifestations and were humanely euthanized using CO_2 based on a score card system (Supplementary Figure 2B). At necropsy, brain and spleens were collected for virus titrations by $CCID_{50}$ assays and/or for histology.

Histopathology and immunohistochemistry

Brains and spleens were fixed in 10% formalin and embedded in paraffin. Human cortical brain organoids were embedded in agarose by adding 4% melted agarose and incubating on ice to solidify, prior to standard paraffin embedding. Sections were stained with H&E (Sigma Aldrich) and slides were scanned using Aperio AT Turbo (Aperio, Vista, CA USA) and analyzed using Aperio ImageScope software (LeicaBiosystems, Mt Waverley, Australia) (v10).

For anti-flavivirus NS1 immunohistochemistry using 4G4, sections were affixed to positively charged adhesive slides and air-dried overnight at 37°C. Sections were dewaxed and rehydrated through xylol and descending graded alcohols to water. Sections were transferred to Dako Epitope Retrieval Solution (pH 9.0) and subjected to heat antigen retrieval (100°C for 20 min) using the Biocare Medical de-cloaking chamber, and slides allowed to cool for 20 minutes before

transferring to TBS plus 0.025% Tween-20 (TBS-T). Endogenous mouse Ig was blocked by incubating sections with donkey anti-mouse Fab fragments (Jackson Immunoresearch) diluted 1:50 in Biocare Medical Rodent block M for 60 minutes. Sections were washed three times in TBS-T, then incubated with anti-mouse Fc for 15 minutes, before a further three washes in TBS-T. Nonspecific antibody binding was inhibited by incubation with Biocare Medical Background Sniper with 1% BSA and 20% donkey serum and 20% goat serum for 15 minutes. Primary antibody 4G4 (mouse anti-flavivirus NS1 [27-29]) was diluted 1 in 4 with Da Vinci Green diluent and applied to the sections overnight at room temperature. Sections were washed three times in TBS-T and endogenous peroxidase was blocked by incubating slides in Biocare Medical Peroxidased 1 for 5 minutes. Sections were washed three times in TBS-T and Perkin Elmer Opal HRP Polymer or Perkin Elmer Goat anti-mouse HRP diluted 1:500 in TBST was applied for 60 minutes. Sections were washed three times in TBS-T and signal developed in Vector Nova Red for 5 minutes after which they were washed three times in water. Sections were lightly counterstained in Haematoxylin (program 7 Leica Autostainer), washed in water, dehydrated through ascending graded alcohols, cleared in xylene, and mounted using DePeX or similar.

Apoptosis was detected using the ApopTag Peroxidase In Situ Apoptosis Detection Kit (Merck Catalogue No. S7100) as per manufacturer's instructions.

For anti-GFAP IHC, antigen retrieval was performed in 0.1M citric acid buffer (pH 6.0) at 1005°C for 20 min. Endogenous peroxidase activity was blocked using 1.0% H_2O_2 and 0.1% sodium azide in TBS for 10 min. Endogenous mouse Ig was blocked by incubating sections with goat anti-mouse Fab fragments (Jackson Immunoresearch) diluted 1:50 in Biocare Medical Mouse block M for 60 minutes. Nonspecific antibody binding was inhibited by incubation with Biocare Medical Background Sniper + 2% BSA for 30 min. Mouse anti-GFAP clone GA-5 (Biocare Medical, CM065C), was diluted 1:250 in the above buffer and incubated on sections for 1 hr at room temperature. After washes, Perkin Elmer Goat anti-mouse HRP diluted 1:500 in TBST was applied for 60 minutes. Nova Red development and counter staining was performed as for 4G4 above.

Infection of human cortical brain organoids

hBOs were reprogrammed from adult dermal fibroblasts (HDFa, Gibco, C0135C) using the CytoTune-iPS 2.0 Sendai Reprogramming Kit (Invitrogen, A16518) [30], and were grown using

the CelVivo Clinostar incubator (Invitro Technologies) as described [31]. On the day of infection, ~30-day-old hBOs were transferred from each Clinoreactor into an ultra-low-binding 24 well plate (one hBO per well), and each hBO was infected with 10^5 $CCID_{50}$ of either $JEV_{Nakayama}$, JEV_{FU}, $JEV_{NSW/22}$, $MVEV_{TC123130}$, Imojev [32], or YFV 17D [29] for ~4 hrs. For shorter term culture (up to 4 days for viral growth kinetics), virus inoculum was removed and hBOs were washed twice with media in the well, before 1 ml differentiation media was added to each well and the 24 well plate was placed within a humidified tissue culture incubator at 37ºC, 5% CO_2 for up to 4 days. For longer term culture (up to 11 dpi), hBOs were washed twice with media by transferring them to an ultra-low-binding 6 well plate containing 5 ml of media, and then hBOs were transferred into 50 mm LUMOX gas exchange dishes (SARSTEDT) (4 organoids per dish) containing 7 ml of differentiation media, and placed within a humidified tissue culture incubator at 37ºC, 5% CO_2 for up to 11 days. hBOs were imaged using an EVOS FL (Advanced Microscopy Group), and organoid area was determined using Image J v1.53 [33].

Statistics

Statistical analyses of experimental data were performed using IBM SPSS Statistics for Windows, Version 19.0 (IBM Corp., Armonk, NY, USA). The t-test was used when the difference in variances was <4, skewness was > -2 and kurtosis was <2. Otherwise, the non-parametric Kolmogorov-Smirnov test was used. Kaplan-Meier statistics were determined by log-rank (Mantel-Cox) test. Area under the curve analysis was performed in GraphPad Prism 8.

Results

$JEV_{NSW/22}$ infection produces a viremia but is not lethal in C57BL/6J mice

The $JEV_{NSW/22}$ G4 virus was isolated from the brain of a stillborn piglet in New South Wales (NSW), Australia in February 2022 (GenBank accession OP904182). The $JEV_{Nakayama}$ G3 prototype was isolated in Japan in 1935 (GenBank accession EF571853), and the JEV_{FU} G2 was isolated in Australia in 1995 [34,35] (GenBank accession AF217620). MVEV was isolated in Australia in 1974 [36] ($MVEV_{TC123130}$, GenBank accession JN119814). The latter three viruses were isolated from human patients. Brief descriptions of the viral isolates and their phylogenic relationships with other flaviviruses are provided in Supplementary Figure 1.

Six week old adult C57BL/6J mice were infected subcutaneously (s.c.) with $5x10^5$ $CCID_{50}$ of

the aforementioned viruses. Viremia for all four viruses were broadly similar, peaking 1 day post infection (dpi) at 2-3 $\log_{10}CCID_{50}$/ml of serum, with nearly all mice showing no detectable viremia by day 4 (Figure 1A-D). Infection appeared to stall weight gain for most mice until day ~10 (Figure 1E). Between 8 to 12 dpi, four mice (2 infected with $JEV_{Nakayama}$, 1 JEV_{FU} and 1 $MVEV_{TC123130}$) out of the total of 24 mice showed weight loss $\geq$20% and were euthanized (Figure 1E, †). A further four mice (1 $JEV_{Nakayama}$, 2 JEV_{FU}, 1 $MVEV_{TC123130}$) lost >5% of their body weight, but subsequently recovered. None of the $JEV_{NSW/22}$ infected mice lost more than ~3% of their body weight (Figure 1E).

Kaplan-Meier survival curves provided no significant differences for the different viral isolates (Figure 1F). Mice that were euthanized also displayed varying levels of abnormal posture (hunching), reduced activity, and fur ruffling, on the day of euthanasia (Supplementary Figure 2A). For the 4 mice that were euthanized (Figure 1E, †) viremias were not overtly higher (Figure 1A-D, open symbols); however, these mice had very high levels of brain infection (≈8-9 $\log_{10}CCID_{50}$/mg) (Figure 1G). At the time of euthanasia, viral titers in the spleen in these mice were below the level of detection (Figure 1G), consistent with the viremia data.

C57BL/6J mice infected with JEV or MVEV led to viral neuroinvasion, apoptosis and reactive astrogliosis

The brains of C57BL/6J mice were analysed by immunohistochemistry (IHC) using the pan-flavivirus anti-NS1 antibody (4G4). Staining was consistently seen in the cortex for JEV and MVEV infected mice, with staining also seen in the thalamus (Figure 2A, Supplementary Figure 3A-C). Prevailing infection of the cerebral cortex and thalamus parallels IHC data from post-mortem human brains [6,37]. In some mice, virus was detected in other brain regions, including the hippocampus, anterior olfactory nucleus (Figure 2A, $JEV_{Nakayama}$), and caudate putamen (Supplementary Figure 3B, JEV_{FU}). A JEV_{FU} infected mouse that lost ~15% body weight and then recovered (Figure 1E) had residual virus staining in the cortex at day 29 post infection (Supplementary Figure 3D), while a mouse that survived infection with minimal weight loss had no detectable viral antigen staining (Supplementary Figure 3E). As expected, 4G4 staining was associated with cells showing neuronal morphology (Figure 2A, Supplementary Figure 3D).

ApopTag staining was evident in areas that were positive for virus staining, particularly in the cortex, and was again associated with cells showing neuronal morphology (Figure 2B and

Supplementary Figure 4A-C). Apoptotic cells were also evident in the mouse that showed ~15% body weight loss and recovered (Supplementary Figure 4D). Mice with signs of disease from JEV or MVEV infection (Supplementary Figure 2) thus showed high levels of viral antigen and apoptosis in the brain. In addition, like in humans, animals can recover from brain infection, despite apoptotic damage, although neurological sequelae may ensue.

Astrocytes are a type of glial cell that provides physical and chemical support to neurons. Astrocytes become activated (reactive astrogliosis) in response to brain pathology, including from JEV infection [38-40]. Reactive astrocytes are characterized by the upregulated expression of glial fibrillary acidic protein (GFAP) and the growth/extension of cellular processes [41]. Brains from mice with signs of disease from JEV or MVEV infection (Supplementary Figure 2) had significant upregulation of GFAP positive astrocytes throughout the brain, including the heavily infected areas of the cortex, thalamus and anterior olfactory nucleus (Figure 2C, Supplementary Figure 5). GFAP is constitutively expressed in astrocytes of the hippocampus, corpus callosum, and cerebral peduncle [42], consistent with staining seen in uninfected brains (Figure 2D, right). Widespread reactive astrogliosis is thus a feature of lethal JEV and MVEV encephalitis in C57BL/6J mice.

IFNAR$^{-/-}$ mice are a model of lethal JEV viremia without neuroinvasion

As $JEV_{NSW/22}$ did not lead to fatal neuroinvasion in C57BL/6J mice, type I interferon receptor knockout (IFNAR$^{-/-}$) mice were evaluated. IFNAR$^{-/-}$ mice have been used extensively in studies of pathogenic flaviviruses such as Zika virus (ZIKV), West Nile virus (WNV), and Yellow fever virus (YFV), and generally provide a robust viremia and a lethal outcome [28,29,43,44]. Adult IFNAR$^{-/-}$ mice were infected with $5x10^5$ $CCID_{50}$ of $JEV_{Nakayama}$, JEV_{FU}, or $JEV_{NSW/22}$ via s.c. injection. A robust viremia developed, reaching 7-8 $log_{10}CCID_{50}$/ml of serum by 2 dpi (Figure 3A). $JEV_{NSW/22}$ infected mice had ≈2 log lower viremia compared to $JEV_{Nakayama}$ and JEV_{FU} on 3 dpi (Figure 3A). Mice displayed a rapid loss of body weight, which was slightly delayed for $JEV_{NSW/22}$ at 2 dpi (Figure 3B), requiring euthanasia 2/3 dpi (Figure 3C). Mice infected with any of the JEV strains also displayed varying levels of abnormal posture (hunching), reduced activity, and fur ruffling (Supplementary Figure 6A).

Consistent with the robust viremia (Figure 3A), spleen tissue titers reached ~6-9 $log_{10}CCID_{50}$/g at 2-3 dpi (Figure 3D). Similar levels were seen in brains (Figure 3E); however,

4G4 staining illustrated that brain cells were not infected (Figure 3F). Viremia and brain titers correlated strongly (Supplementary Figure 6B), arguing that the brain titers (Figure 3E) arose from virus in the blood vessels of the brain. Interestingly, anti-flavivirus NS1 antibody staining was clearly present in blood vessels (Figure 3G,H), with extracellular JEV NS1 also found in serum of JEV patients [45]. NS1 from JEV is reported to increase vascular leakage and may contribute to mortality [46], although overt vascular leakage was not evident in H&E sections of brains at 2-3 dpi. Neither apoptosis (Supplementary Figure 6C), nor significantly increased staining for reactive astrocytes (Supplementary Figure 5, IFNAR$^{-/-}$) were apparent for brains of JEV-infected IFNAR$^{-/-}$ mice.

JEV$_{NSW/22}$ is less virulent than JEV$_{Nakayama}$ and JEV$_{FU}$ in IRF7$^{-/-}$ mice

C57BL/6J mice had a relatively low viremia and low penetrance of lethal brain infection (Figure 1), and IFNAR$^{-/-}$ mice had a rapid and lethal viremia without brain infection (Figure 3). A model with a higher penetrance of brain infection is clearly desirable, given encephalitis is the key clinical concern for JEV infections. Interferon regulatory factor 7 knockout (IRF7$^{-/-}$ mice) were thus chosen as these mice produced an intermediate phenotype for WNV [47], as well as another arbovirus [24]. As lower inoculation doses of JEV were reported to increase mortality [48], adult C57BL/6J and IRF7$^{-/-}$ mice were inoculated s.c. with JEV$_{NSW/22}$ at 5x10^4, 5x10^3 and 5x10^2 CCID$_{50}$. Reducing the dose of JEV$_{NSW/22}$ for C57BL/6J mouse infection (compared to the 5x10^5 dose used in Figure 1) did not provide significant changes to weight change or viremia (Supplementary Figure 7A, C-E). For JEV$_{NSW/22}$ infection in IRF7$^{-/-}$ mice, the inoculation dose of 5x10^3 CCID$_{50}$ provided a peak viremia 2 dpi that was marginally higher than the other doses tested (Figure 4C, Supplementary Figure 7F-G). One mouse infected with this dose had weight loss >20% requiring euthanasia on 8 dpi, whereas the 5x10^2 and 5x10^4 infection doses caused weight loss no greater than ≈10% (Supplementary Figure 7B). An inoculation dose of 5x10^3 CCID$_{50}$ was thus chosen for IRF7$^{-/-}$ mice.

JEV$_{NSW/22}$, JEV$_{Nakayama}$ and JEV$_{FU}$ infection of IRF7$^{-/-}$ mice (dose 5x10^3 CCID$_{50}$) resulted in robust viremias (Figure 4A-C), that were higher than those seen in C57BL/6J mice, where the dose was 5x10^5 CCID$_{50}$ (Figure 1A-C). Area under the curve analysis indicated no significant difference between the viremias for the three JEV strains in IRF7$^{-/-}$ mice. MVEV$_{TC123130}$ infection produced a viremia in all IRF7$^{-/-}$ mice, although area under the curve analysis indicated

viremias were significantly lower than JEV (Figure 4D).

Infection of IRF7$^{-/-}$ mice with the different JEV isolates and MVEV (n=10 mice per group) illustrated a mean weight loss of 3-12% for all four groups (Figure 4E), with the exception of 15 mice that reached ethically defined end points for weight loss and/or disease manifestations (Supplementary Figure 8). Kaplan-Meier curves illustrated significantly higher survival for IRF7$^{-/-}$ mice infected with JEV$_{NSW/22}$ when compared with JEV$_{Nakayama}$ and JEV$_{FU}$, with only 1/10 IRF7$^{-/-}$ mice infected with JEV$_{NSW/22}$ requiring euthanasia (Figure 4F). MVEV$_{TC123130}$ showed no lethality in IRF7$^{-/-}$ mouse (Figure 4F), consistent with the low viremia (Figure 4D).

Brain infection in IRF7$^{-/-}$ mice infected with JEV

Brains titers in euthanized IRF7$^{-/-}$ mice were ~4-9 log$_{10}$CCID$_{50}$/gram, while spleen titers were <2-5 log$_{10}$CCID$_{50}$/g (Figure 4G). IHC staining for viral antigen confirmed JEV infection in the brains of IRF7$^{-/-}$ mice (Figure 4H), with reduced levels of staining reflecting lower brain titers (Supplementary Figure 9). Viral antigen staining was consistently present in the cortex, with staining also seen in the medulla, thalamus, and hippocampus (Figure 4H-I, Supplementary Figure 9). Brain regions showing ApopTag staining broadly overlapped with staining for viral antigen (Figure 4H-I). Reactive astrogliosis was also evident (Supplementary Figure 5). Overall, this suggests that JEV infection of IRF7$^{-/-}$ mice produced a consistent viremia, with mice showing brain infection and apoptotic damage.

JEV causes severe histological lesions in C57BL/6J and IRF7$^{-/-}$ mouse brains

H&E staining of JEV infected mouse brains revealed a series of histopathological lesions, predominantly neuronal degeneration, neuronal vacuolation, perivascular cuffing, leukocyte infiltrates, hemorrhage, meningitis and microgliosis (Figure 5A). IHC for the microglial marker, Iba1, confirmed the presence microgliosis (Figure 5B).

The presence of H&E lesions were scored for the different JEV isolates and mouse strains (Supplementary Figure 10). C57BL/6J and IRF7$^{-/-}$ mice euthanized during acute infections had a broadly similar incidence of the aforementioned lesions, whereas only hemorrhage was seen in IFNAR$^{-/-}$ mice (Supplementary Figure 10, Acute). Neuronal degeneration, neuronal vacuolation, hemorrhage and microgliosis was not seen in the n=1 JEV$_{NSW/22}$ infected IRF7$^{-/-}$ mouse that was euthanized 8 dpi (Supplementary Figure 10, Acute). For C57BL/6J and IRF7$^{-/-}$ mice that

survived and were euthanized later (nominally chronic phase), only hemorrhage was consistently observed (Supplementary Figure 10, Chronic).

Lesions in C57BL/6J and IRF7$^{-/-}$ mouse brains were associated with areas of high virus infection, most prominently in the cortex (Supplementary Figure 11); however, lesions were also found in other areas of the brain including where there was minimal viral antigen staining (Supplementary Figure 12A). Some mice that lost >8% body weight and then recovered had persistent lesions detectable at the latest time point sampled (up to day 32 for C57BL/6J and day 19 for IRF7$^{-/-}$) (Supplementary Figure 12B), consistent with persistent neurological sequelae in humans that survive infection. Mice that did not lose any body weight did not show any overt brain lesions at the later time points, indicating that brain infection causing weight loss is associated with persistent lesions.

Overall, the lesions in C57BL/6J and IRF7$^{-/-}$ mouse brains are consistent with H&E detectable lesions in post-mortem human JEV infected brains [6,38,49-51].

Publically available RNA-Seq data of mouse brains infected with JEV

A publically available RNA-Seq data (raw read counts) of C57BL/6 brain infection with JEV isolate P20778 (Vellore strain, genotype 3)[52] (GEO accession: GSE154002) was reanalyzed [53] to provide a list of differentially expressed genes (DEGs) for infected brains versus uninfected brains from C57BL/6 mice. GFAP was significantly up-regulated 5.4 fold by infection (Supplementary Table 2, $\log_2$FC 2.4), consistent with the GFAP IHC (Figure 2C) and reactive astrogliosis seen herein. Iba1 (Aif1) was also significantly up-regulated 5.5 fold (Supplementary Table 2, $\log_2$FC 2.5), consistent with the H&E and IHC (Figure 5) and microgliosis observed in our study. To provide potential insights into the nature of the cellular infiltrates (e.g. perivascular cuffing and leukocyte infiltrates, Figure 5), immune cell type abundance estimates were obtained from the aforementioned RNA-Seq expression data using SpatialDecon [54]. The dominant cell types identified were CD4 T cells, NKT cells, monocytes/macrophages, neutrophils, innate lymphoid cells, T regs, and CD8 T cells, with an increase in microglia cells also identified (Supplementary Figure 13).

Productive replication of JEV in human cortical brain organoids

Human cortical brain organoids (hBOs) have been used to investigate the pathogenesis of

flaviviruses, including JEV and ZIKV [44,55,56]. We generated ~30 day old hBO from HDFa cells, growing the "minibrains" in a CelVivo Clinostar incubator as described [31] (Figure 6A). hBOs were infected with 10^5 $CCID_{50}$ of the indicated JEV and MVEV isolates, as well as (i) the Imojev chimeric virus vaccine (previously called ChimeriVax-JE) comprising the prME genes of JEV on the YFV 17D backbone [32,57] and (ii) the Yellow Fever live attenuated vaccine strain (YFV 17D) [29], with wild-type YFV infection [58], and occasionally YFV 17D vaccination [59], able to cause neuropathology. hBOs were fixed in formalin 4 dpi and IHC undertaken using the anti-NS1 monoclonal antibody 4G4 [29]. $JEV_{Nakayama}$ infected hBOs showed the most pronounced viral antigen staining, with $JEV_{NSW/22}$, JEV_{FU} and $MVEV_{TC123130}$ also showing clear staining (Figure 6B). Viral antigen was primarily localized to the outer surface of the organoids (Figure 6B), where cells are in direct contact with the culture medium. Viral antigen staining for Imojev and YFV 17D infected hBOs was also seen, but was sparse (Figure 6B and Supplementary Figure 14A).

All viruses were able to productively infect hBOs, with $JEV_{Nakayama}$ infection generating higher viral titers than Imojev at all time points (Figure 6C, $p<0.001$). By 96 h $JEV_{Nakayama}$ titers were also significantly higher than those seen for $JEV_{NSW/22}$ (Figure 6C).

Over 11 days, uninfected hBOs grew in size by ~20% (Figure 6D, Uninfected). hBOs infected with JEV isolates shrank in cross sectional area by ~5% to 15% by 11 dpi, although when compared with uninfected organoids, this only approached significance for $JEV_{NSW/22}$ (Figure 6D; Supplementary Figure 14B-C). hBOs infected with $MVEV_{TC123130}$, Imojev and YFV 17D infected hBO did not shrink significantly when compared with uninfected controls, although the $MVEV_{TC123130}$ data suggested a marginal reduction in area (Figure 6C; Supplementary Figure 14C). These data (Figure 6D) mirror viral replication data (Figure 6C) and likely reflect virus-induced CPE.

All viruses replicated productively in a human neural progenitor cell line, RENcell VM, with all viruses except Imojev causing fulminant CPE (Supplementary Figure 15A,B). Although Vero E6 cells are widely used for flavivirus research, CPE induced by $JEV_{NSW/22}$ was considerably less pronounced in these cells (Supplementary Figure 15C).

Discussion

Herein we provide a comprehensive *in vivo* and *in vitro* characterization of the genotype 4

$JEV_{NSW/22}$ isolate from the recent Australian outbreak, and illustrate mouse models of infection and CNS neuropathological manifestations that recapitulate many aspects of human and primates disease [6,37-40,60]. Like the proptypical JEV_{FU} (G2) and $JEV_{Nakayama}$ (G3) isolates, $JEV_{NSW/22}$ was able productively to infect hBOs, and in $IRF7^{-/-}$ mice, retained the capacity for neuroinvasive infection, generation of severe histopathological lesions and induction of mortality, consistent with reported human fatalities in the 2022 Australian outbreak.

Serosurvey data, albeit limited, suggests the ratio of human symptomatic to asymptomatic infections is not particularly different for $JEV_{NSW/22}$. To date 45 clinical cases have been notified for the recent outbreak in Australia [61], with serosurveys in Victoria (n=820 participants) and New South Wales (NSW) (n=917 participants) reporting 3.3% and 8.7% of participants as seropositive for JEV, respectively [62,63]. Although somewhat dated, population data for the primary recruitment locations for the serosurveys is available from Australian Bureau of Statistics 2016, with Victorian recruitment locations providing a population total of 160,294 (Mildura, Lockington, Shepparton, Cobram, Yarrawonga, Rutherglen, Wodonga, Wangaratta, Rochester), and NSW locations a total of 68,431 (Balranald, Corowa, Dubbo, Griffith, Temora). As [0.033 x 160,294] + [0.087 x 68,431] / 250 = 45, the serosurvey data is consistent with the expected symptomatic to asymptomatic ratio of ≈1 in 250 for JEV and thus provides no compelling evidence for virulence differences for $JEV_{NSW/22}$ in human populations.

Mouse models of flavivirus pathogenesis frequently use $IFNAR^{-/-}$ mice [29,64,65] as flaviviruses often replicate poorly in wild-type mice as the ability of NS5 to suppress the antiviral type I IFN responses in humans often fails to operate in mice [66]. We show herein that $IFNAR^{-/-}$ mice are not a good model for JEV neuropathology, as they reach ethically defined endpoints before brain infection can occur. However $IFNAR^{-/-}$ mice are a good model of robust and lethal viremia, which may provide a useful and stringent model for vaccine testing. $IRF7^{-/-}$ mice do provide a new and useful model for JEV as they show high penetrance of brain infection and neuropathology after s.c. inoculation of JEV. $IRF7^{-/-}$ retain the ability to induce some type I IFN responses (primarily via IRF3) [24] that likely prevent early mortality, thereby allowing subsequent brain infection. $JEV_{NSW/22}$ showed lower levels of mortality than JEV_{FU} and $JEV_{Nakayama}$ in $IRF7^{-/-}$ mice (Figure 4F). $JEV_{NSW/22}$ also showed less pronounced induction of CPE in Vero E6 cells (Supplementary Figure 15C), another system in which type I interferon responses are diminished. Vero E6 cells retain the ability to respond to IFNα/β, but cannot make type I IFNs

[67]. These results suggest $JEV_{NSW/22}$ is more sensitive to, or less able to suppress, type I IFN responses. Inhibition of type I IFN responses is mediated by NS5 for inhibition of STAT2 and NS3 [68] and subgenomic flavivirus RNA (sfRNA)/NS5 [44] for inhibition of STAT1. Although the latter likely operates for WNV in mice [69] and is involved in promoting apoptosis [44], the efficiency of these systems during JEV infection of humans and mice remains to be determined. sfRNA is derived from the 3'UTR [44], where $JEV_{NSW/22}$ does show a small number of nucleic acid changes that are unlikely to affect sfRNA production (Supplementary Table 1).

$JEV_{NSW/22}$ does not contain known attenuating mutations that would explain its reduced virulence in $IRF7^{-/-}$ mice. There are 9 amino acids in the Imojev vaccine envelope gene that have been associated with attenuated neurovirulence; F107, K138, V176, A177, G244, H264, M279, V315 and R439 [70-80]. At these positions, $JEV_{Nakayama}$, JEV_{FU}, $JEV_{NSW/22}$, and $MVEV_{TC123130}$ all have the same amino acids (L107, E138, T177, E244, Q264, K279, A315, and K439), except for position 176 where $JEV_{Nakayama}$ has T176, and JEV_{FU}, $JEV_{NSW/22}$, and $MVEV_{TC123130}$ have I176 (Supplementary Table 1). $JEV_{NSW/22}$ retains E at position 138, and this amino acid has been identified by several studies as a principal neurovirulence determinant [81-85], with a role in neuronal cell binding hypothesized [86]. YFV 17D has a valine (V) at this residue, possibly contributing to reduced neurovirulence [87]. NS1 and NS2A have been implicated in neuroinvasion, but not neurovirulence [79]. Among the six changes in NS1 associated with attenuation of neuroinvasiveness are R147H and R339M [79], of which H147 is present in both $JEV_{Nakayama}$ and $JEV_{NSW/22}$, with K339 (a conserved substitution for R) present in $JEV_{NSW/22}$. JEV non-structural protein 4B (NS4B) alone can induce apoptosis and encephalitis [88], however, NS4B is completely conserved between $JEV_{Nakayama}$, JEV_{FU}, and $JEV_{NSW/22}$ (Supplementary Table 1). prM has been reported to influence neuroinvasiveness of ZIKV [64] and JEV virulence in mice [89]. $JEV_{NSW/22}$ has a number of unique changes in prM (Supplementary Table 1), although their functional implications remain unclear. $JEV_{NSW/22}$ also has an additional N-linked glycosylation site at position 175 in NS1 that is lacking in $JEV_{Nakayama}$ and JEV_{FU} (Supplementary Table 1). However, this N-linked glycosylation site is reported to increase WNV neuroinvasiveness in wild-type mice [90,91], a trend not seen in our JEV data (Figure 1F). Thus $JEV_{NSW/22}$ shows no obvious sequence characteristics that can be ready associated with reduced virulence.

Limitations of this study include the use of $JEV_{NSW/22}$, a pig isolate; however, there are only 4

amino acid differences between this isolate and a JEV G4 sequence from a human brain in the Tiwi Islands (Northern Territory, Australia) in 2021 (Genbank accession OM867669} [17]). The differences are; envelope-238 F vs. L, NS2A-71 I vs. T, NS2B-59 E vs. G, NS3-436 E vs. G. In addition, $JEV_{Nakayama}$ was passaged in suckling mouse brains, which may contribute to the increased neuroinvasion seen herein, although the adaptive mutations acquired during passaging, if any, are currently unknown. Furthermore, JEV_{FU} has not been passaged in mice, but was still more lethal than $JEV_{Nakayama}$ in $IRF7^{-/-}$ mice. Use of C57BL/6J mice that lack a functional nicotinamide nucleotide transhydrogenase *(Nnt)* may be another issue, as background and *Nnt* are able to affect viral immunopathogenesis [25,53]. However, we found that neither *Nnt* nor a C57BL/6N genetic background significantly impacted JEV replication or immunopathology (Supplementary Figure 16).

In conclusion, we show that $JEV_{NSW/22}$ retains capacity for robust replication in neurons, and is capable of neuroinvasive infection, severe histopathological lesions and mortality in $IRF7^{-/-}$ mice, consistent with reported human fatalities in the 2022 Australian outbreak.

ACKNOWLEDGEMENTS

From QIMR Berghofer MRI we thank Dr I Anraku for managing the PC3 (BSL3) facility, animal house staff for mouse breeding and agistment, Drs Anthony White and Lotta Oikari for providing the iPSC line, Crystal Chang, Sang-Hee Park andAshwini Potadar for the histology and immunohistochemistry, Dr Viviana Lutzky for proof reading. We thank Dr. Peter Kirkland for supplying the $JEV_{NSW/22}$ isolate. We thank Dr. Andrii Slonchak for insights into whether 3’UTR changes may affect sfRNA production.

DATA AVAILABILITY

All data is provided in the manuscript and accompanying supplementary files.

FUNDING

A.S. holds an Investigator grant from the National Health and Medical Research Council (NHMRC) of Australia (APP1173880). We also acknowledge the intramural grant from QIMR Berghofer awarded to R.S. and D.J.R. for purchase of the CelVivo Clinostar incubator.

AUTHOR CONTRIBUTIONS

Conceptualization, D.J.R. Methodology, D.J.R., W.N., and A.S. Formal analysis, W.N., D.J.R. and A.S. Investigation, W.N., B.T., R.S., K.Y., N.G., T.L., and D.J.R. Resources, R.S., N.G., G.D., and A.S. Data curation, W.N., D.J.R., and A.S. Writing, original draft – D.J.R. Writing, review and editing, A.S and W.N. Visualization, D.J.R., W.N. and A.S. Supervision, D.J.R., G.D. and A.S. Project administration, D.J.R., G.D. and A.S. Funding acquisition, D.J.R, G.D. and A.S.

DECLARATION OF INTERESTS

The authors declare no competing interests.

FIGURE LEGENDS

Figure 1. JEV and MVEV infection in C57BL/6J mice. (A-D) Female ≈6 week old C57BL/6J mice were infected s.c. with $5x10^5$ $CCID_{50}$ of the indicated viruses. Viremia for each of the n=6 per group over 6 days is shown. Horizontal lines show mean viremia ± SE. All mice recorded a detectable viremia for at least one timepoint. Limit of detection is 2 $log_{10}CCID_{50}$/ml of serum. Open symbols indicate the viremia of mice that were euthanized due to weight loss reaching the ethically defined endpoint of ≥20%. (E) Percent body weight change of individual mice compared to each mouse's weight on day zero. Four mice lost ≥20% body weight and were euthanized (†). (F) Kaplan-Meier plot showing percent survival (n=6 for each virus/virus isolate). (G) Viral tissue titers in brains and spleens of the four euthanized mice (n=2 $JEV_{Nakayama}$, n=1 JEV_{FU}, n=1 $MVEV_{TC123130}$). Tissue titers determined by $CCID_{50}$ assay (limit of detection ~2 $log_{10}CCID_{50}$/g).

Figure 2. IHC for viral antigen, apoptosis and reactive astrocytes in JEV infected C57BL/6J mouse brain. IHC of $JEV_{Nakayama}$ infected brain (required euthanasia on 9 dpi, brain virus titer 9.2 $log_{10}CCID_{50}$/g). (A) Staining for flavivirus NS1 using the 4G4 monoclonal antibody. High magnification images show cells with neuronal morphology in the cortex (left) and hippocampus (right). The latter also shows staining of dendrites and axons (fibrilar patterns above and densely staining cells). 4G4 staining of brains of the other mice requiring euthanasia (marked by † in Figure 1E) is shown in Supplementary Figure 3. (B) ApopTag staining of the

same brain as in 'A'. High magnification images show cells with neuronal morphology in the cortex (left) and apoptotic cells in the dentate gyrus (right). ApopTag staining of the brains of the other mice requiring euthanasia is shown in Supplementary Figure 4. (C) Staining for GFAP, a marker of reactive astrocytes, for the same brain as in 'A'. High magnification images show a typical reactive astrocyte in the cortex (left) and reactive astrocytes in the thalamus (right). GFAP IHC for the brains of the other mice requiring euthanasia is shown in Supplementary Figure 5. (D) IHC negative controls; uninfected mouse brain stained with 4G4 (left), ApopTag (middle), and anti-GFAP (right).

Figure 3. JEV lethal viremia in IFNAR$^{-/-}$ mice. Female IFNAR$^{-/-}$ mice (9-24 week old) were infected s.c. with $5x10^5$ $CCID_{50}$ of the indicated virus (n=4 per group). (A) Mean viremia determined by $CCID_{50}$ assay (limit of detection 2 $log_{10}CCID_{50}$/ml). Statistics by t-tests. (B) Mean percent body weight change compared to 0 dpi. Statistics 2 dpi $JEV_{NSW/22}$ versus $JEV_{Nakayama}$ (Kolmogorov-Smirnov test, p=0.023) and for $JEV_{NSW/22}$ versus JEV_{FU} (t-test, p=0.008). (C) Kaplan-Meier plot showing percent survival. (D) Viral tissue titers in spleens harvested at euthanasia (3 dpi for all mice except for 1 JEV_{FU} mouse at 2 dpi), determined by $CCID_{50}$ assay (limit of detection ~2 log_{10} $CCID_{50}$/g). (E) Viral titers in brains. (F) IHC staining for flavivirus NS1 using the 4G4 monoclonal antibody. (G, H) High magnification images from F showing NS1 staining in blood vessels surrounding the pale grey, biconcave shaped, red blood cells.

Figure 4. JEV neuroinvasive infection in IRF7$^{-/-}$ mice. IRF7$^{-/-}$ mice (15-48 weeks old) were infected s.c. with $5x10^3$ $CCID_{50}$ of the indicated virus. (A-D) Viremias for indicated virus determined by $CCID_{50}$ assay; limit of detection is 2 $log_{10}CCID_{50}$/ml. Horizontal line indicates mean at each time point, and error bars represent SE; n=4 mice per group. Unfilled symbols represent data for mice that were euthanized due to acute disease manifestations (Supplementary Figure 8). (E) Percent body weight change compared to 0 dpi. Four mice lost >20% body weight were euthanized (marked by †) and are plotted individually. The weight change for the remaining mice are shown as means $\pm$ SE. Data is from two independent experiments, n=10 mice per group. (F) Kaplan-Meier plot showing percent survival (n=10 per group, data from two independent experiments). Statistics by log-rank (Mantel-Cox) tests. Symbols as for E. (G)

Brain and spleen tissue titers for 8 euthanized mice (n=3 $JEV_{Nakayama}$, n=4 JEV_{FU}, n=1 $JEV_{NSW/22}$). Tissue titers determined by $CCID_{50}$ assay (limit of detection ~2 $log_{10}CCID_{50}$/g). (H) IHC of $JEV_{NSW/22}$ infected brain (euthanized on day 8, brain virus titer 6.3 $log_{10}CCID_{50}$/g) using 4G4 monoclonal antibody (top) or ApopTag (bottom). High magnification images of cortex (left) and medulla (right). (I) IHC using 4G4 (left) and ApopTag IHC (right) for the $JEV_{Nakayama}$ infected brain with the highest virus titer (euthanized on day 7, brain virus titer 8.3 $log_{10}CCID_{50}$/g). IHC using 4G4 for the brains of two other euthanized mice are shown in Supplementary Figure 9.

Figure 5. Histological lesions in brains of JEV infected mice. (A) Examples of indicated lesions stained with H&E. Degeneration of neurons indicated by (i) pyknotic nuclei (black unfilled arrow heads indicating condensation and fragmentation of nuclei, staining dark blue), and (ii) hyper-eosinophilic cytoplasm of degenerating neurons in the cornus ammonis of the hippocampus (area also staining for viral antigen Supplementary Figure 11). Neuronal vacuolation indicated by fluid accumulation around the neurons (arrowheads). Perivascular cuffing is indicated by leukocytes aggregating in blood vessels (arrowheads). Leukocyte infiltrates (extravascular) are indicated by dashed ovals. Hemorrhagic lesions are indicated by extravascular red blood cells (arrows). Microgliosis is indicated by accumulation of microglia, which have an elongated rod-shaped nuclei (arrows). Meningitis is indicated by accumulation of leukocytes around the meninges (arrowheads). Images of uninfected controls accompany each image(s) of lesions. (B) IHC using anti-Iba1, a microglial marker.

Figure 6. Infection of human cortical brain organoids (hBOs). (A) Photograph of "mini-brains" cultured in a rotating CelVivo Clinostar incubator. (B) IHC of viral antigen (4G4) for hBOs at 4 dpi. Images are representative of n=4 hBOs for each group. Magnified images of sparse Imojev and YFV 17D infected cells are shown in Supplementary Figure 13A. (B) Viral growth kinetics determined by $CCID_{50}$ assays of culture supernatants at the indicated hours post infection; limit of detection is 2 $log_{10}CCID_{50}$/ml. At all time points $JEV_{Nakayama}$ vs. Imojev, and at 96 h $JEV_{Nakayama}$ vs. $JEV_{NSW/22}$ were significant (t tests, n=5 organoids per group). (C) Mean percentage change in organoid area 11 dpi vs. 9 dpi for each organoid (n=8 for uninfected and $MVEV_{TC123130}$, otherwise n=4). Statistics are by Kolmogorov-Smirnov test for uninfected versus

$JEV_{Nakayama}$, and t-test for uninfected versus JEV_{FU} or $JEV_{NSW/22}$.

References

1 van den Hurk, A. F., Ritchie, S. A. & Mackenzie, J. S. Ecology and Geographical Expansion of Japanese Encephalitis Virus. *Annual Review of Entomology* **54**, 17-35, doi:10.1146/annurev.ento.54.110807.090510 (2008).

2 Ashraf, U. *et al.* Pathogenicity and virulence of Japanese encephalitis virus: Neuroinflammation and neuronal cell damage. *Virulence* **12**, 968-980, doi:10.1080/21505594.2021.1899674 (2021).

3 Solomon, T. *et al.* Japanese encephalitis. *Journal of Neurology, Neurosurgery & Psychiatry* **68**, 405, doi:10.1136/jnnp.68.4.405 (2000).

4 Quan, T. M., Thao, T. T. N., Duy, N. M., Nhat, T. M. & Clapham, H. Estimates of the global burden of Japanese encephalitis and the impact of vaccination from 2000-2015. *eLife* **9**, e51027, doi:10.7554/eLife.51027 (2020).

5 Hsieh, J. T., Rathore, A. P. S., Soundarajan, G. & St John, A. L. Japanese encephalitis virus neuropenetrance is driven by mast cell chymase. *Nat Commun* **10**, 706, doi:10.1038/s41467-019-08641-z (2019).

6 Johnson, R. T. *et al.* Japanese encephalitis: immunocytochemical studies of viral antigen and inflammatory cells in fatal cases. *Ann Neurol* **18**, 567-573, doi:10.1002/ana.410180510 (1985).

7 Hegde, N. R. & Gore, M. M. Japanese encephalitis vaccines: Immunogenicity, protective efficacy, effectiveness, and impact on the burden of disease. *Hum Vaccin Immunother* **13**, 1-18, doi:10.1080/21645515.2017.1285472 (2017).

8 Pham, D. *et al.* Emergence of Japanese encephalitis in Australia: a diagnostic perspective. *Pathology* **54**, 669-677, doi:10.1016/j.pathol.2022.07.001 (2022).

9 Bharucha, T. *et al.* Mouse models of Japanese encephalitis virus infection: A systematic review and meta-analysis using a meta-regression approach. *PLOS Neglected Tropical Diseases* **16**, e0010116, doi:10.1371/journal.pntd.0010116 (2022).

10 Beasley, D. W. C. *et al.* Protection against Japanese encephalitis virus strains representing four genotypes by passive transfer of sera raised against ChimeriVax™-JE experimental vaccine. *Vaccine* **22**, 3722-3726, doi:https://doi.org/10.1016/j.vaccine.2004.03.027 (2004).

11 Tajima, S. *et al.* Growth, Pathogenesis, and Serological Characteristics of the Japanese Encephalitis Virus Genotype IV Recent Strain 19CxBa-83-Cv. *Viruses* **15**, 239 (2023).

12 Gao, X. *et al.* Changing Geographic Distribution of Japanese Encephalitis Virus Genotypes, 1935-2017. *Vector Borne Zoonotic Dis* **19**, 35-44, doi:10.1089/vbz.2018.2291 (2019).

13 Kang, B. K. *et al.* Comparison of the antigenic relationship between Japanese encephalitis virus genotypes 1 and 3. *Clin Exp Vaccine Res* **5**, 26-30, doi:10.7774/cevr.2016.5.1.26 (2016).

14 Han, N. *et al.* Comparison of genotypes I and III in Japanese encephalitis virus reveals distinct differences in their genetic and host diversity. *J Virol* **88**, 11469-11479, doi:10.1128/jvi.02050-14 (2014).

15 Mulvey, P. *et al.* The Ecology and Evolution of Japanese Encephalitis Virus. *Pathogens* **10**, doi:10.3390/pathogens10121534 (2021).

16 Lee, A. R., Song, J. M. & Seo, S. U. Emerging Japanese Encephalitis Virus Genotype V in Republic of Korea. *J Microbiol Biotechnol* **32**, 955-959, doi:10.4014/jmb.2207.07002 (2022).

17 Sikazwe, C. *et al.* Molecular detection and characterisation of the first Japanese encephalitis virus belonging to genotype IV acquired in Australia. *PLoS Negl Trop Dis* **16**, e0010754, doi:10.1371/journal.pntd.0010754 (2022).

18 Mackenzie, J. S., Williams, D. T., van den Hurk, A. F., Smith, D. W. & Currie, B. J. Japanese Encephalitis Virus: The Emergence of Genotype IV in Australia and Its Potential Endemicity. *Viruses* **14** (2022).

19 Yakob, L. *et al.* Japanese encephalitis emergence in Australia: the potential population at risk. *Clin Infect Dis*, doi:10.1093/cid/ciac794 (2022).

20 Gyawali, N. *et al.* Neglected Australian Arboviruses Associated With Undifferentiated Febrile Illnesses. *Front Microbiol* **10**, 2818, doi:10.3389/fmicb.2019.02818 (2019).

21 Johnson, B. J. *et al.* Heat shock protein 10 inhibits lipopolysaccharide-induced inflammatory mediator production. *J Biol Chem* **280**, 4037-4047, doi:10.1074/jbc.M411569200 (2005).

22 Honda, K. *et al.* IRF-7 is the master regulator of type-I interferon-dependent immune responses. *Nature* **434**, 772-777, doi:10.1038/nature03464 (2005).

23 Sato, M. *et al.* Distinct and essential roles of transcription factors IRF-3 and IRF-7 in response to viruses for IFN-alpha/beta gene induction. *Immunity* **13**, 539-548, doi:10.1016/s1074-7613(00)00053-4 (2000).

24 Rudd, P. A. *et al.* Interferon response factors 3 and 7 protect against Chikungunya virus hemorrhagic fever and shock. *J Virol* **86**, 9888-9898, doi:10.1128/JVI.00956-12 (2012).

25 Rawle, D. J. *et al.* Widespread discrepancy in Nnt genotypes and genetic backgrounds complicates granzyme A and other knockout mouse studies. *eLife* **11**, e70207, doi:10.7554/eLife.70207 (2022).

26 Dumenil, T. *et al.* Warmer ambient air temperatures reduce nasal turbinate and brain infection, but increase lung inflammation in the K18-hACE2 mouse model of COVID-19. *Science of The Total Environment* **859**, 160163, doi:https://doi.org/10.1016/j.scitotenv.2022.160163 (2023).

27 Prow, N. A. *et al.* A vaccinia-based single vector construct multi-pathogen vaccine protects against both Zika and chikungunya viruses. *Nat Commun* **9**, 1230, doi:10.1038/s41467-018-03662-6 (2018).

28 Hobson-Peters, J. *et al.* A recombinant platform for flavivirus vaccines and diagnostics using chimeras of a new insect-specific virus. *Science Translational Medicine* **11**, eaax7888, doi:10.1126/scitranslmed.aax7888 (2019).

29 Yan, K. *et al.* A Yellow Fever Virus 17D Infection and Disease Mouse Model Used to Evaluate a Chimeric Binjari-Yellow Fever Virus Vaccine. *Vaccines* **8** (2020).

30 Oikari, L. E. *et al.* Altered Brain Endothelial Cell Phenotype from a Familial Alzheimer Mutation and Its Potential Implications for Amyloid Clearance and Drug Delivery. *Stem Cell Reports* **14**, 924-939, doi:10.1016/j.stemcr.2020.03.011 (2020).

31 Stewart, R. *et al.* Increased neurovirulence of omicron BA.5 over BA.1 in human brain organoids and K18-hACE2 mice. PREPRINT (Version 1) Research Square https://doi.org/10.21203/rs.3.rs-2702556/v1. (2023).

32 Guirakhoo, F. *et al.* Immunogenicity, genetic stability, and protective efficacy of a recombinant, chimeric yellow fever-Japanese encephalitis virus (ChimeriVax-JE) as a live, attenuated vaccine candidate against Japanese encephalitis. *Virology* **257**, 363-372, doi:10.1006/viro.1999.9695 (1999).

33 Schneider, C. A., Rasband, W. S. & Eliceiri, K. W. NIH Image to ImageJ: 25 years of image analysis. *Nature Methods* **9**, 671-675, doi:10.1038/nmeth.2089 (2012).

34 Williams, D. T., Wang, L. F., Daniels, P. W. & Mackenzie, J. S. Molecular characterization of the first Australian isolate of Japanese encephalitis virus, the FU strain. *J Gen Virol* **81**, 2471-2480, doi:10.1099/0022-1317-81-10-2471 (2000).

35 Poidinger, M., Hall, R. A. & Mackenzie, J. S. Molecular Characterization of the Japanese Encephalitis Serocomplex of the Flavivirus Genus. *Virology* **218**, 417-421, doi:https://doi.org/10.1006/viro.1996.0213 (1996).

697 36 Williams, D. T. *et al.* The Molecular Epidemiology and Evolution of Murray Valley Encephalitis
698 Virus: Recent Emergence of Distinct Sub-lineages of the Dominant Genotype 1. *PLOS Neglected*
699 *Tropical Diseases* **9**, e0004240, doi:10.1371/journal.pntd.0004240 (2015).
700 37 Iwasaki, Y., Zhao, J. X., Yamamoto, T. & Konno, H. Immunohistochemical demonstration of viral
701 antigens in Japanese encephalitis. *Acta Neuropathol* **70**, 79-81, doi:10.1007/bf00689518 (1986).
702 38 German, A. C. *et al.* A preliminary neuropathological study of Japanese encephalitis in humans
703 and a mouse model. *Trans R Soc Trop Med Hyg* **100**, 1135-1145,
704 doi:10.1016/j.trstmh.2006.02.008 (2006).
705 39 Siva Venkatesh, I. P., Bhaskar, M. & Basu, A. Japanese encephalitis viral infection modulates
706 proinflammatory cyto/chemokine profile in primary astrocyte and cell line of astrocytic origin.
707 *Metabolic Brain Disease* **37**, 1487-1502, doi:10.1007/s11011-022-00991-w (2022).
708 40 Li, Y. *et al.* Microarray Analysis Identifies the Potential Role of Long Non-Coding RNA in
709 Regulating Neuroinflammation during Japanese Encephalitis Virus Infection. *Frontiers in*
710 *Immunology* **8**, doi:10.3389/fimmu.2017.01237 (2017).
711 41 Wilhelmsson, U. *et al.* Redefining the concept of reactive astrocytes as cells that remain within
712 their unique domains upon reaction to injury. *Proceedings of the National Academy of Sciences*
713 **103**, 17513-17518, doi:10.1073/pnas.0602841103 (2006).
714 42 Zhang, Z. *et al.* The Appropriate Marker for Astrocytes: Comparing the Distribution and
715 Expression of Three Astrocytic Markers in Different Mouse Cerebral Regions. *BioMed Research*
716 *International* **2019**, 9605265, doi:10.1155/2019/9605265 (2019).
717 43 Hazlewood, J. E. *et al.* The Chimeric Binjari-Zika Vaccine Provides Long-Term Protection against
718 ZIKA Virus Challenge. *Vaccines (Basel)* **10**, doi:10.3390/vaccines10010085 (2022).
719 44 Slonchak, A. *et al.* Zika virus noncoding RNA cooperates with the viral protein NS5 to inhibit
720 STAT1 phosphorylation and facilitate viral pathogenesis. *Science Advances* **8**, eadd8095,
721 doi:10.1126/sciadv.add8095 (2022).
722 45 Roberts, A., Kesarwani, V., Gupta, R. & Gandhi, S. Electroactive reduced graphene oxide for
723 highly sensitive detection of secretory non-structural 1 protein: A potential diagnostic biomarker
724 for Japanese encephalitis virus. *Biosens Bioelectron* **198**, 113837,
725 doi:10.1016/j.bios.2021.113837 (2022).
726 46 Puerta-Guardo, H. *et al.* Flavivirus NS1 Triggers Tissue-Specific Vascular Endothelial Dysfunction
727 Reflecting Disease Tropism. *Cell Reports* **26**, 1598-1613.e1598,
728 doi:https://doi.org/10.1016/j.celrep.2019.01.036 (2019).
729 47 Daffis, S. *et al.* Interferon regulatory factor IRF-7 induces the antiviral alpha interferon response
730 and protects against lethal West Nile virus infection. *J Virol* **82**, 8465-8475,
731 doi:10.1128/jvi.00918-08 (2008).
732 48 Aoki, K. *et al.* Type-I interferon response affects an inoculation dose-independent mortality in
733 mice following Japanese encephalitis virus infection. *Virology Journal* **11**, 105, doi:10.1186/1743-
734 422X-11-105 (2014).
735 49 Miyake, M. THE PATHOLOGY OF JAPANESE ENCEPHALITIS. A REVIEW. *Bull World Health Organ*
736 **30**, 153-160 (1964).
737 50 Waller, C. *et al.* Japanese Encephalitis in Australia — A Sentinel Case. *New England Journal of*
738 *Medicine* **387**, 661-662, doi:10.1056/NEJMc2207004 (2022).
739 51 Maamary, J. *et al.* New Detection of Locally Acquired Japanese Encephalitis Virus Using Clinical
740 Metagenomics, New South Wales, Australia. *Emerging Infectious Disease journal* **29**, 627,
741 doi:10.3201/eid2903.220632 (2023).
742 52 Tripathi, A. *et al.* Lack of Interferon (IFN) Regulatory Factor 8 Associated with Restricted IFN-
743 gamma Response Augmented Japanese Encephalitis Virus Replication in the Mouse Brain. *J Virol*
744 **95**, e0040621, doi:10.1128/JVI.00406-21 (2021).

745 53 Bishop, C. R. *et al.* Mouse models of COVID-19 recapitulate inflammatory pathways rather than
746 gene expression. *PLoS Pathog* **18**, e1010867, doi:10.1371/journal.ppat.1010867 (2022).
747 54 Danaher, P. *et al.* Advances in mixed cell deconvolution enable quantification of cell types in
748 spatial transcriptomic data. *Nat Commun* **13**, 385, doi:10.1038/s41467-022-28020-5 (2022).
749 55 Setoh, Y. X. *et al.* Determinants of Zika virus host tropism uncovered by deep mutational
750 scanning. *Nat Microbiol* **4**, 876-887, doi:10.1038/s41564-019-0399-4 (2019).
751 56 Zhang, B. *et al.* Differential antiviral immunity to Japanese encephalitis virus in developing
752 cortical organoids. *Cell Death & Disease* **9**, 719, doi:10.1038/s41419-018-0763-y (2018).
753 57 Chambers, T. J., Nestorowicz, A., Mason, P. W. & Rice, C. M. Yellow fever/Japanese encephalitis
754 chimeric viruses: construction and biological properties. *J Virol* **73**, 3095-3101,
755 doi:10.1128/jvi.73.4.3095-3101.1999 (1999).
756 58 Frassetto, F. P. & Rosemberg, S. Neuropathology of yellow fever autopsy cases. *Tropical*
757 *Diseases, Travel Medicine and Vaccines* **9**, 1, doi:10.1186/s40794-022-00187-1 (2023).
758 59 Cohen, M. *et al.* Case Report: Yellow Fever Vaccine-Associated Neurotropic Disease and
759 Associated MRI, EEG, and CSF Findings. *Front Neurol* **12**, 779014,
760 doi:10.3389/fneur.2021.779014 (2021).
761 60 Myint, K. S. *et al.* Neuropathogenesis of Japanese encephalitis in a primate model. *PLoS Negl*
762 *Trop Dis* **8**, e2980, doi:10.1371/journal.pntd.0002980 (2014).
763 61 Japanese encephalitis virus (JEV). Australian Governement Dept of Health and Aged Care.
764 https://www.health.gov.au/health-alerts/japanese-encephalitis-virus-jev/japanese-encephalitis-
765 virus-jev (accessed April 2023).
766 62 Serourvey for JEV in northern Victoria. https://www.health.vic.gov.au/infectious-
767 diseases/serosurvey-for-japanese-encephalitis-in-northern-victoria (accessed April 2023).
768 63 Summary of NSW JEV seosurvey results.
769 https://www.health.nsw.gov.au/environment/pests/vector/Documents/jev-serosurvey-
770 report.pdf (accessed April 2023).
771 64 Nakayama, E. *et al.* Neuroinvasiveness of the MR766 strain of Zika virus in IFNAR-/- mice maps
772 to prM residues conserved amongst African genotype viruses. *PLoS Pathog* **17**, e1009788,
773 doi:10.1371/journal.ppat.1009788 (2021).
774 65 Zheng, W. *et al.* Liver transcriptomics reveals features of the host response in a mouse model of
775 dengue virus infection. *Front Immunol* **13**, 892469, doi:10.3389/fimmu.2022.892469 (2022).
776 66 Grant, A. *et al.* Zika Virus Targets Human STAT2 to Inhibit Type I Interferon Signaling. *Cell Host*
777 *Microbe* **19**, 882-890, doi:10.1016/j.chom.2016.05.009 (2016).
778 67 Prow, N. A. *et al.* Lower temperatures reduce type I interferon activity and promote alphaviral
779 arthritis. *PLoS Pathog* **13**, e1006788, doi:10.1371/journal.ppat.1006788 (2017).
780 68 Setoh, Y. X. *et al.* Helicase Domain of West Nile Virus NS3 Protein Plays a Role in Inhibition of
781 Type I Interferon Signalling. *Viruses* **9**, 326 (2017).
782 69 Laurent-Rolle, M. *et al.* The NS5 protein of the virulent West Nile virus NY99 strain is a potent
783 antagonist of type I interferon-mediated JAK-STAT signaling. *J Virol* **84**, 3503-3515,
784 doi:10.1128/JVI.01161-09 (2010).
785 70 Yang, H. *et al.* A novel amino acid site closely associated with the neurovirulence of live,
786 attenuated Japanese encephalitis vaccine (SA14-14-2 strain). *Vaccine* **38**, 2636-2642,
787 doi:https://doi.org/10.1016/j.vaccine.2020.01.005 (2020).
788 71 Yun, S. I. *et al.* A molecularly cloned, live-attenuated japanese encephalitis vaccine SA14-14-2
789 virus: a conserved single amino acid in the ij Hairpin of the Viral E glycoprotein determines
790 neurovirulence in mice. *PLoS Pathog* **10**, e1004290, doi:10.1371/journal.ppat.1004290 (2014).

791 72 Arroyo, J. *et al.* Molecular basis for attenuation of neurovirulence of a yellow fever
792 Virus/Japanese encephalitis virus chimera vaccine (ChimeriVax-JE). *J Virol* **75**, 934-942,
793 doi:10.1128/jvi.75.2.934-942.2001 (2001).
794 73 Yang, D. *et al.* Characterization of live-attenuated Japanese encephalitis vaccine virus SA14-14-2.
795 *Vaccine* **32**, 2675-2681, doi:https://doi.org/10.1016/j.vaccine.2014.03.074 (2014).
796 74 Liu, X. *et al.* The structure differences of Japanese encephalitis virus SA14 and SA14-14-2 E
797 proteins elucidate the virulence attenuation mechanism. *Protein & Cell* **10**, 149-153,
798 doi:10.1007/s13238-018-0551-6 (2019).
799 75 Yang, J. *et al.* Envelope Protein Mutations L107F and E138K Are Important for Neurovirulence
800 Attenuation for Japanese Encephalitis Virus SA14-14-2 Strain. *Viruses* **9** (2017).
801 76 Ni, H., Chang, G. J., Xie, H., Trent, D. W. & Barrett, A. D. Molecular basis of attenuation of
802 neurovirulence of wild-type Japanese encephalitis virus strain SA14. *J Gen Virol* **76 (Pt 2)**, 409-
803 413, doi:10.1099/0022-1317-76-2-409 (1995).
804 77 Zhou, Y. *et al.* Mutation of I176R in the E coding region weakens Japanese encephalitis virus
805 neurovirulence, but not its growth rate in BHK-21 cells. *Arch Virol* **163**, 1351-1355,
806 doi:10.1007/s00705-018-3765-2 (2018).
807 78 Anwar, M. N. *et al.* Phenotypic and Genotypic Comparison of a Live-Attenuated Genotype I
808 Japanese Encephalitis Virus SD12-F120 Strain with Its Virulent Parental SD12 Strain. *Viruses* **12**
809 (2020).
810 79 Gromowski, G. D., Firestone, C. Y. & Whitehead, S. S. Genetic Determinants of Japanese
811 Encephalitis Virus Vaccine Strain SA14-14-2 That Govern Attenuation of Virulence in Mice. *J Virol*
812 **89**, 6328-6337, doi:10.1128/jvi.00219-15 (2015).
813 80 Monath, T. P. *et al.* Single mutation in the flavivirus envelope protein hinge region increases
814 neurovirulence for mice and monkeys but decreases viscerotropism for monkeys: relevance to
815 development and safety testing of live, attenuated vaccines. *J Virol* **76**, 1932-1943,
816 doi:10.1128/jvi.76.4.1932-1943.2002 (2002).
817 81 Chen, L. K. *et al.* Generation and characterization of organ-tropism mutants of Japanese
818 encephalitis virus in vivo and in vitro. *Virology* **223**, 79-88, doi:10.1006/viro.1996.0457 (1996).
819 82 Sumiyoshi, H., Tignor, G. H. & Shope, R. E. Characterization of a highly attenuated Japanese
820 encephalitis virus generated from molecularly cloned cDNA. *J Infect Dis* **171**, 1144-1151,
821 doi:10.1093/infdis/171.5.1144 (1995).
822 83 Zheng, X. *et al.* Acidity/Alkalinity of Japanese Encephalitis Virus E Protein Residue 138 Alters
823 Neurovirulence in Mice. *J Virol* **92**, doi:10.1128/jvi.00108-18 (2018).
824 84 Chiou, S. S. & Chen, W. J. Phenotypic changes in the Japanese encephalitis virus after one
825 passage in Neuro-2a cells: generation of attenuated strains of the virus. *Vaccine* **26**, 15-23,
826 doi:10.1016/j.vaccine.2007.10.047 (2007).
827 85 Zhao, Z. *et al.* Characterization of the E-138 (Glu/Lys) mutation in Japanese encephalitis virus by
828 using a stable, full-length, infectious cDNA clone. *J Gen Virol* **86**, 2209-2220,
829 doi:10.1099/vir.0.80638-0 (2005).
830 86 Wang, X. *et al.* Near-atomic structure of Japanese encephalitis virus reveals critical determinants
831 of virulence and stability. *Nature Communications* **8**, 14, doi:10.1038/s41467-017-00024-6
832 (2017).
833 87 Xia, Q. *et al.* Virulence and Cross-Protection Conferred by an Attenuated Genotype I-Based
834 Chimeric Japanese Encephalitis Virus Strain Harboring the E Protein of Genotype V in Mice.
835 *Microbiology Spectrum* **10**, e01990-01922, doi:10.1128/spectrum.01990-22 (2022).
836 88 Wang, Q. *et al.* Japanese Encephalitis Virus Induces Apoptosis and Encephalitis by Activating the
837 PERK Pathway. *J Virol* **93**, doi:10.1128/jvi.00887-19 (2019).

838 89 Tajima, S. *et al.* E and prM proteins of genotype V Japanese encephalitis virus are required for its
839 increased virulence in mice. *Heliyon* **5**, e02882, doi:10.1016/j.heliyon.2019.e02882 (2019).
840 90 Whiteman, M. C. *et al.* Multiple amino acid changes at the first glycosylation motif in NS1
841 protein of West Nile virus are necessary for complete attenuation for mouse neuroinvasiveness.
842 *Vaccine* **29**, 9702-9710, doi:10.1016/j.vaccine.2011.09.036 (2011).
843 91 Whiteman, M. C. *et al.* Development and characterization of non-glycosylated E and NS1 mutant
844 viruses as a potential candidate vaccine for West Nile virus. *Vaccine* **28**, 1075-1083,
845 doi:10.1016/j.vaccine.2009.10.112 (2010).

846

Figure 1

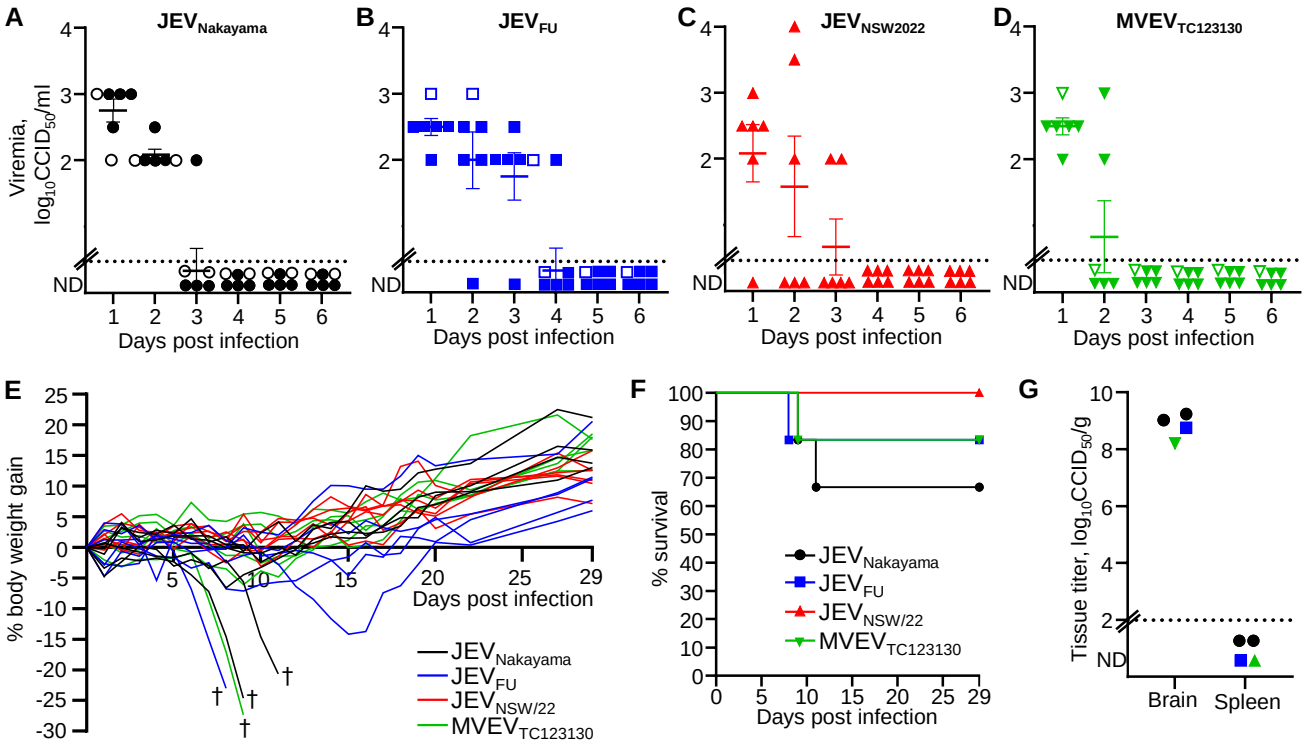
A
JEVNakayama
Viremia, log10CCID50/ml
ND
Days post infection
B
JEVFU
C
JEVNSW2022
D
MVEVTC123130
E
% body weight gain
Days post infection
JEVNakayama
JEVFU
JEVNSW/22
MVEVTC123130
F
% survival
Days post infection
G
Tissue titer, log10CCID50/g
Brain
Spleen

Figure 2

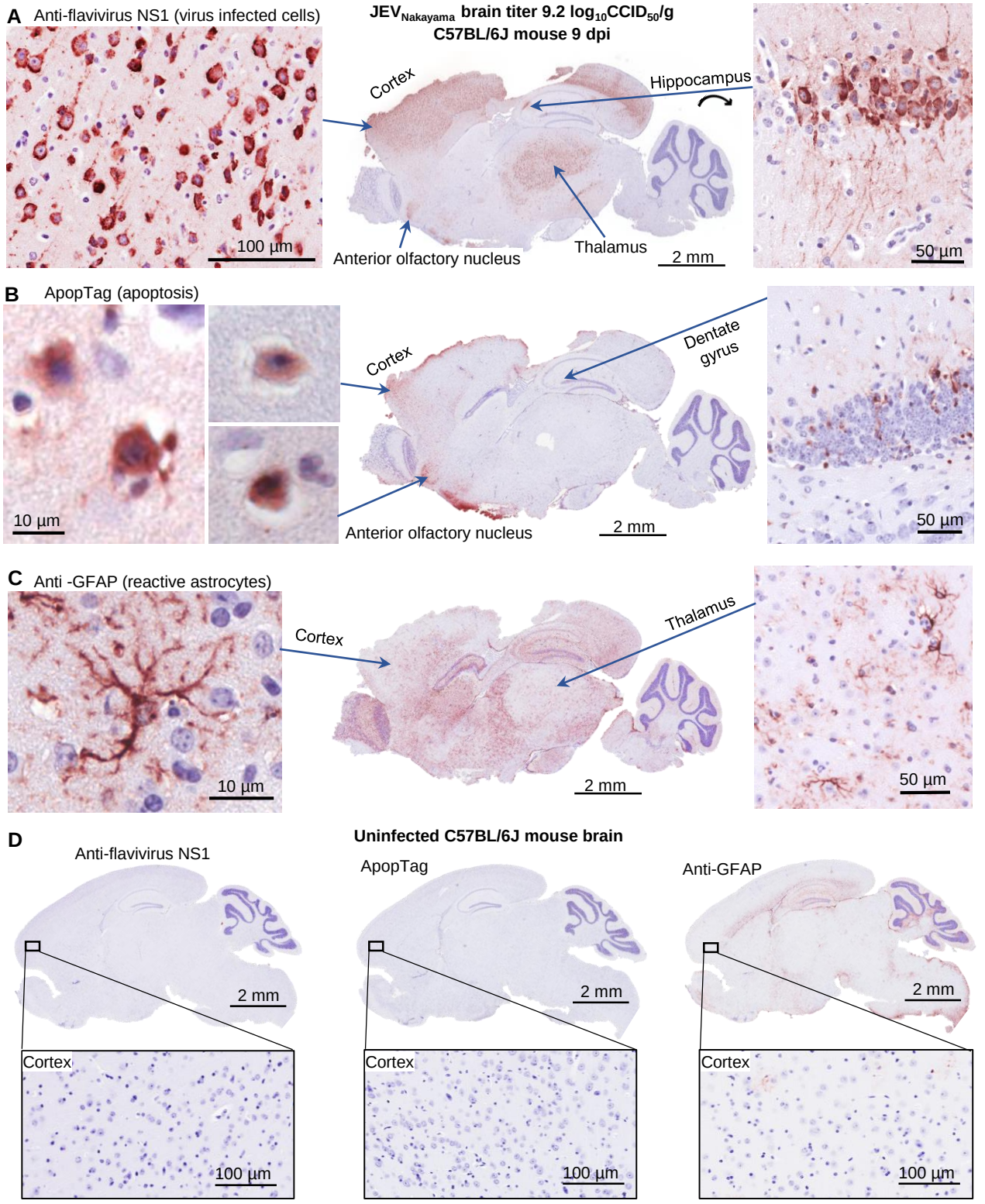
A
Anti-flavivirus NS1 (virus infected cells)
JEV$_{Nakayama}$ brain titer 9.2 log$_{10}$CCID$_{50}$/g
C57BL/6J mouse 9 dpi
Cortex
Hippocampus
Thalamus
Anterior olfactory nucleus
100 µm
2 mm
50 µm
B
ApopTag (apoptosis)
Cortex
Dentate gyrus
Anterior olfactory nucleus
10 µm
2 mm
50 µm
C
Anti -GFAP (reactive astrocytes)
Cortex
Thalamus
10 µm
2 mm
50 µm
D
Uninfected C57BL/6J mouse brain
Anti-flavivirus NS1
ApopTag
Anti-GFAP
2 mm
Cortex
100 µm

Figure 3

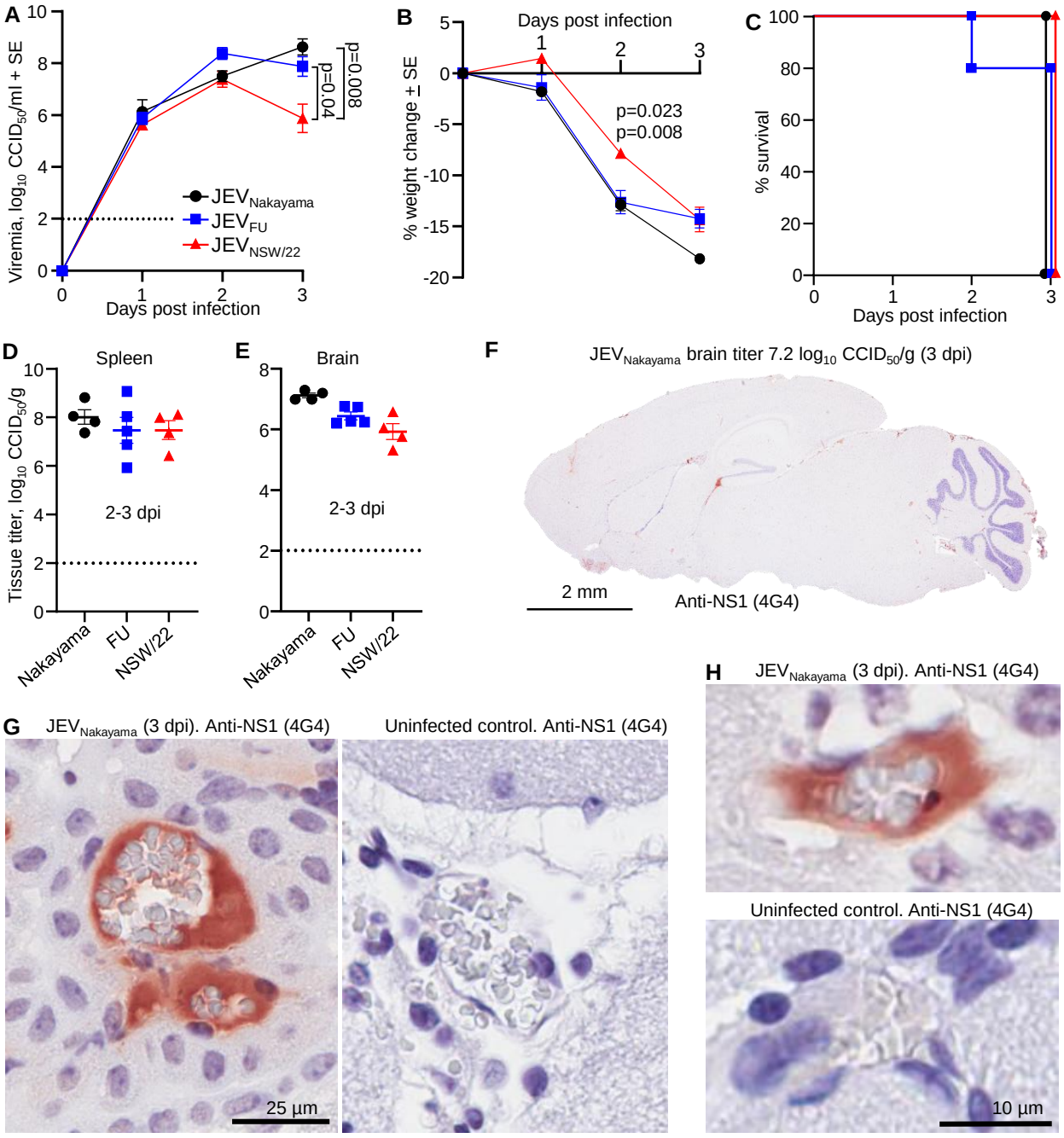
A
Viremia, log10 CCID50/ml + SE
Days post infection
JEVNakayama
JEVFU
JEVNSW/22
p=0.04
p=0.008
B
Days post infection
% weight change ± SE
p=0.023
p=0.008
C
% survival
Days post infection
D
Spleen
Tissue titer, log10 CCID50/g
2-3 dpi
Nakayama
FU
NSW/22
E
Brain
2-3 dpi
Nakayama
FU
NSW/22
F
JEVNakayama brain titer 7.2 log10 CCID50/g (3 dpi)
2 mm
Anti-NS1 (4G4)
G
JEVNakayama (3 dpi). Anti-NS1 (4G4)
Uninfected control. Anti-NS1 (4G4)
25 µm
H
JEVNakayama (3 dpi). Anti-NS1 (4G4)
Uninfected control. Anti-NS1 (4G4)
10 µm

Figure 4

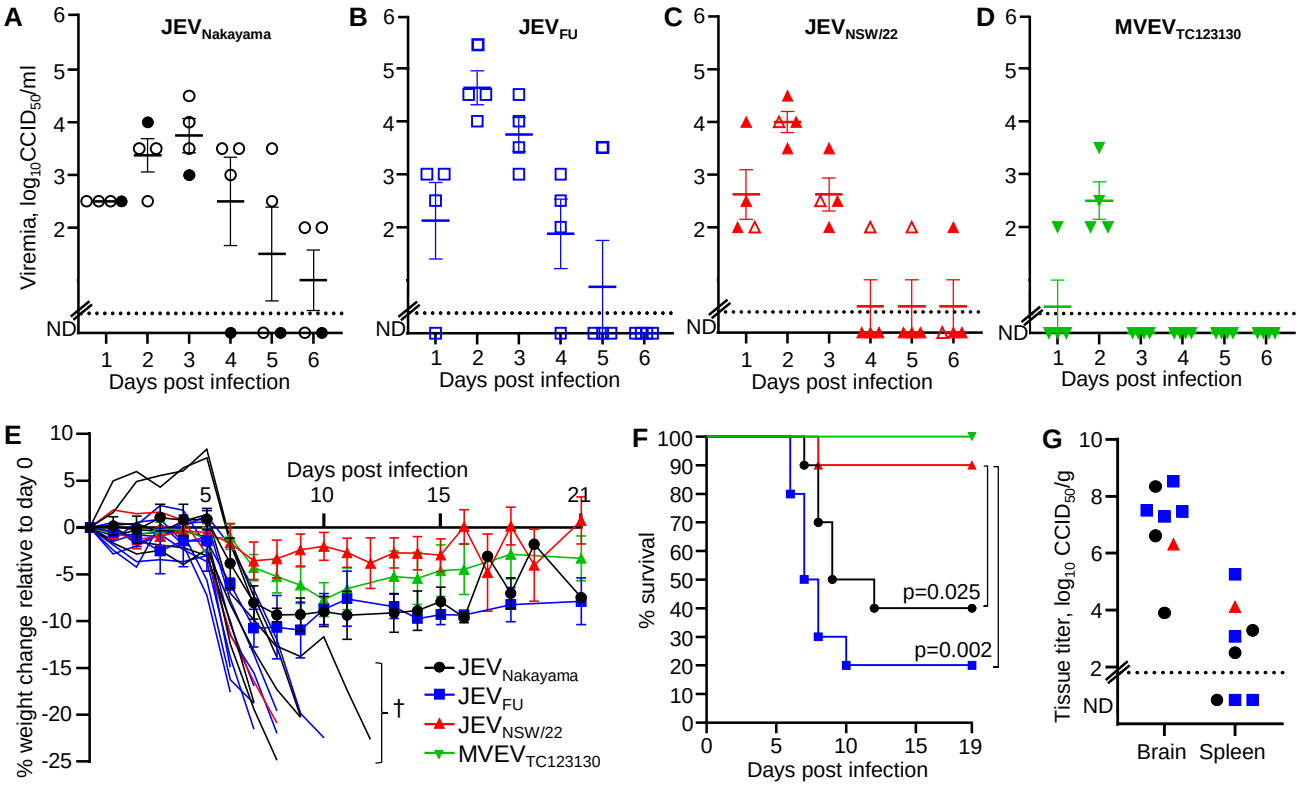
A
JEVNakayama
Viremia, log10CCID50/ml
ND
Days post infection
B
JEVFU
C
JEVNSW/22
D
MVEVTC123130
E
% weight change relative to day 0
Days post infection
JEVNakayama
JEVFU
JEVNSW/22
MVEVTC123130
F
% survival
p=0.025
p=0.002
Days post infection
G
Tissue titer, log10 CCID50/g
Brain
Spleen

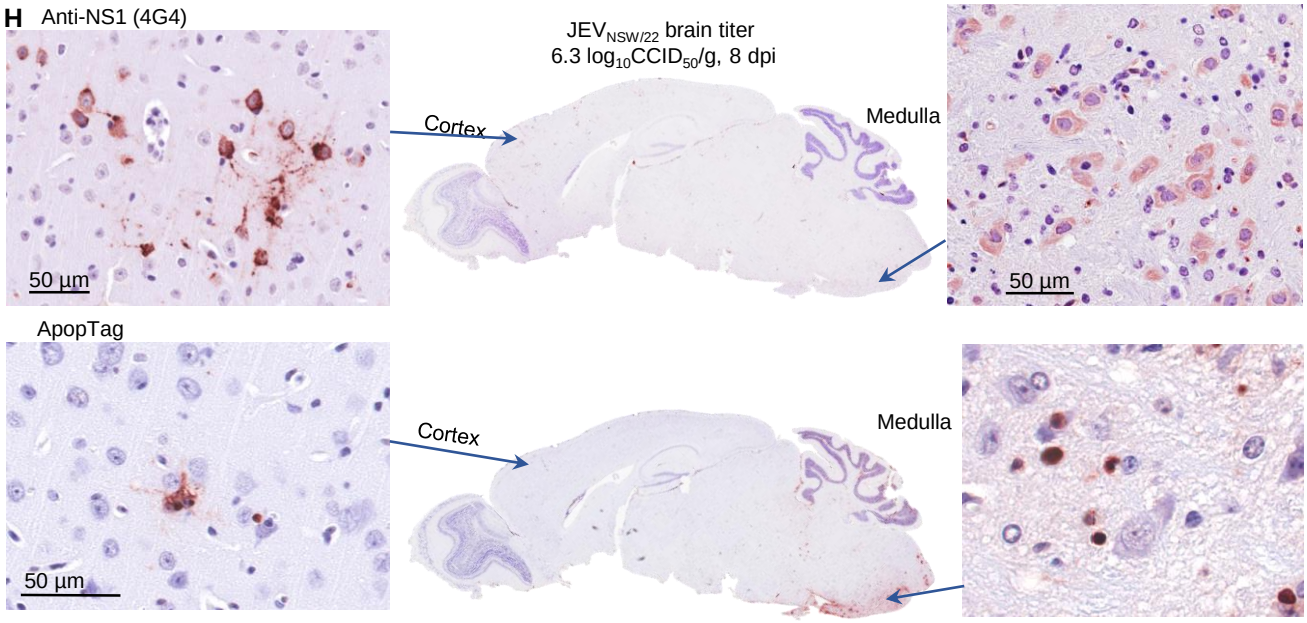
H
Anti-NS1 (4G4)
JEVNSW/22 brain titer
6.3 log10CCID50/g, 8 dpi
Cortex
Medulla
50 µm
ApopTag
50 µm

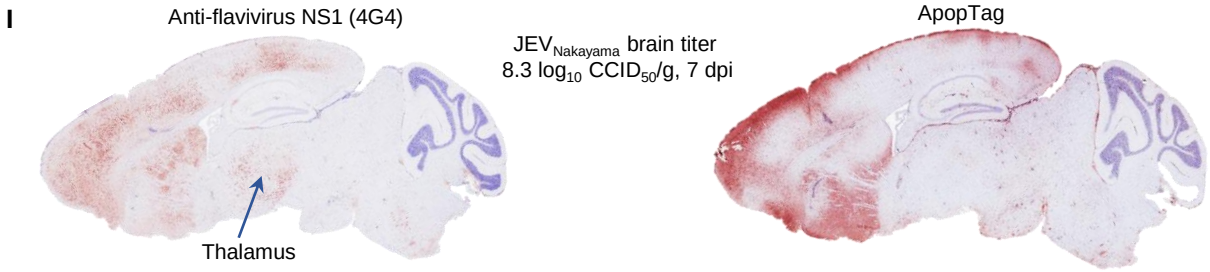
I
Anti-flavivirus NS1 (4G4)
JEVNakayama brain titer
8.3 log10 CCID50/g, 7 dpi
ApopTag
Thalamus

Figure 5

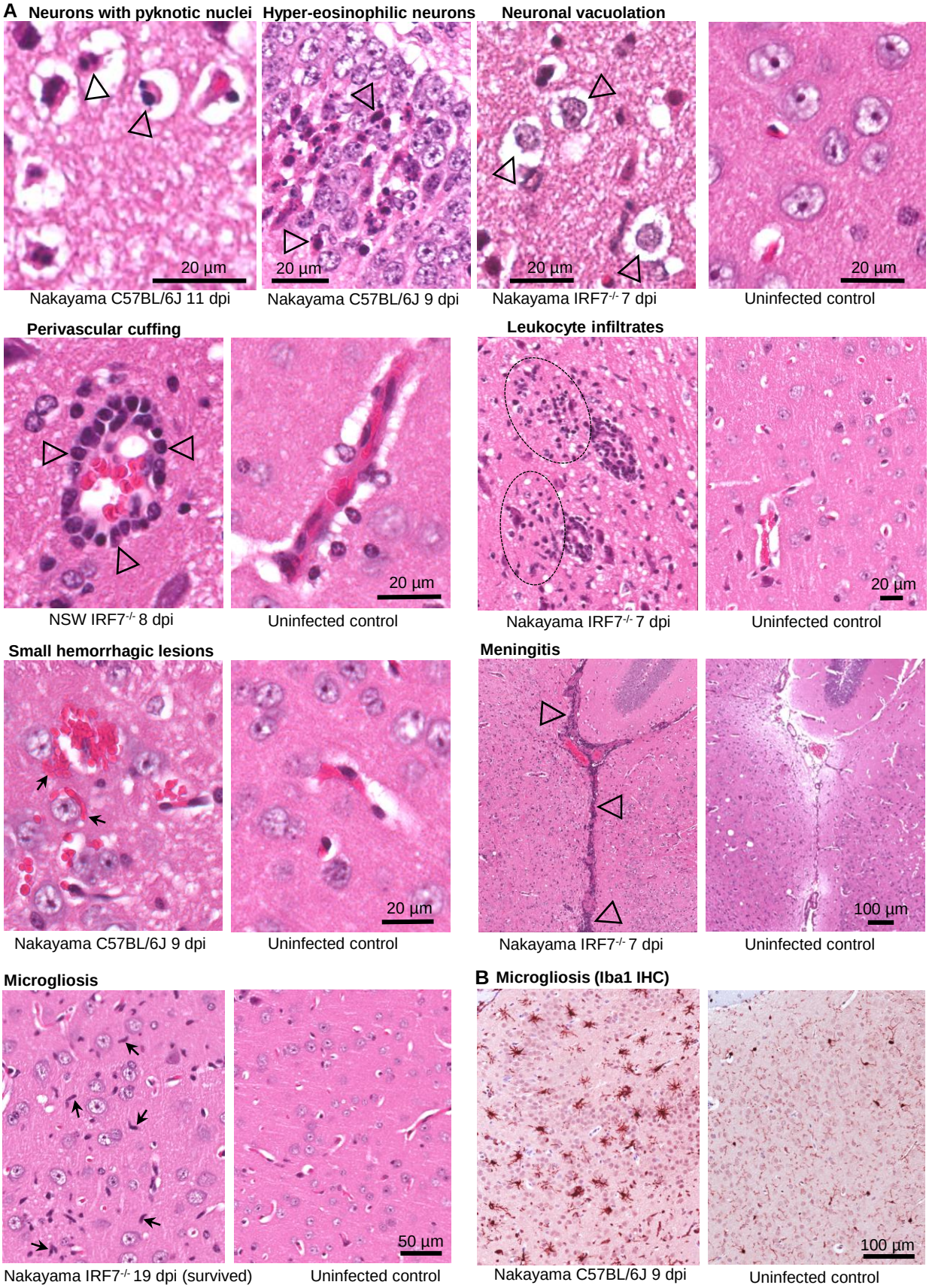
A
Neurons with pyknotic nuclei
Hyper-eosinophilic neurons
Neuronal vacuolation
20 µm
20 µm
20 µm
20 µm
Nakayama C57BL/6J 11 dpi
Nakayama C57BL/6J 9 dpi
Nakayama IRF7-/- 7 dpi
Uninfected control
Perivascular cuffing
Leukocyte infiltrates
20 µm
20 µm
NSW IRF7-/- 8 dpi
Uninfected control
Nakayama IRF7-/- 7 dpi
Uninfected control
Small hemorrhagic lesions
Meningitis
20 µm
100 µm
Nakayama C57BL/6J 9 dpi
Uninfected control
Nakayama IRF7-/- 7 dpi
Uninfected control
Microgliosis
B Microgliosis (Iba1 IHC)
50 µm
100 µm
Nakayama IRF7-/- 19 dpi (survived)
Uninfected control
Nakayama C57BL/6J 9 dpi
Uninfected control

Figure 6

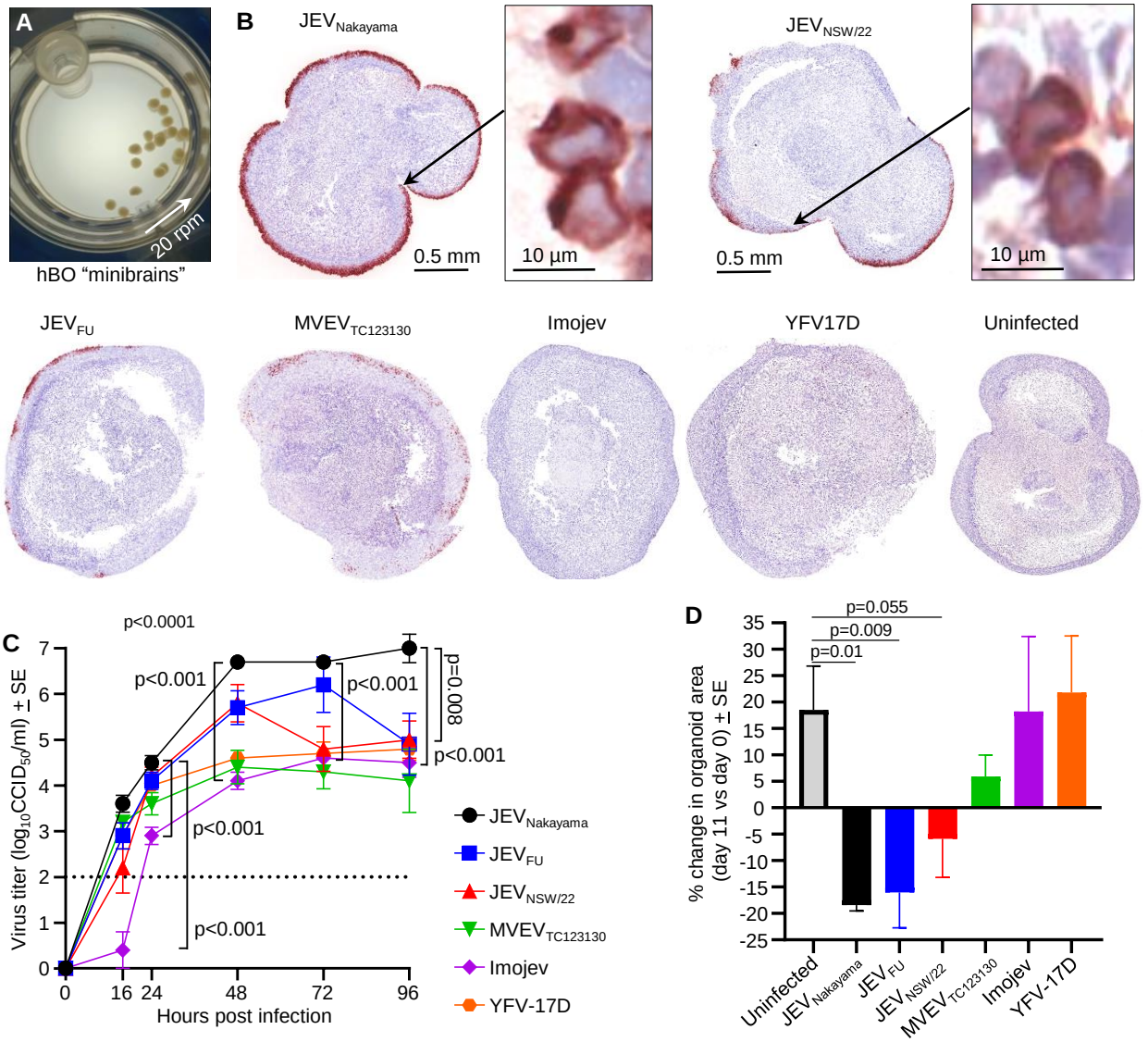
A
20 rpm
hBO "minibrains"
B
JEV Nakayama
0.5 mm
10 µm
JEV NSW/22
0.5 mm
10 µm
JEV FU
MVEV TC123130
Imojev
YFV17D
Uninfected
C
p<0.0001
p<0.001
p<0.001
p=0.008
p<0.001
p<0.001
p<0.001
Virus titer (log10CCID50/ml) ± SE
Hours post infection
JEV Nakayama
JEV FU
JEV NSW/22
MVEV TC123130
Imojev
YFV-17D
D
p=0.055
p=0.009
p=0.01
% change in organoid area (day 11 vs day 0) ± SE
Uninfected
JEV Nakayama
JEV FU
JEV NSW/22
MVEV TC123130
Imojev
YFV-17D

A

Virus name	GenBank accession	JEV Genotype	Isolation year	Isolation source	Passage history
$JEV_{Nakayama}$	EF571853	3	1935	Human cerebrospinal fluid	>11 x suckling mouse brain
JEV_{FU}	AF217620	2	1995	Human serum	C6/36 (unknown number)
$JEV_{NSW2022}$	OP904182	4	2022	Stillborn piglet brain	1 x C6/36 1 x BHK-21
$MVEV_{TC123130}$	JN119814	N/A	1974	Human brain	Unknown
YFV 17D	MT107250	N/A	1927 (Original "Asibi" parent isolate)	Human serum (Original "Asibi" parent isolate)	53 x monkeys 18 x embryonic mouse tissue 50 x minced whole chicken embryo 152 x nervous tissue deprived chick embryo
JEV_{prME} component in Imojev (SA_{14}-14-2 strain)	MK585066	3	1954 (Original SA-14 parent isolate)	*Culex pipiens* mosquito larvae (Original SA-14 parent isolate)	100 x primary hamster kidney cells 22 x suckling mice

B

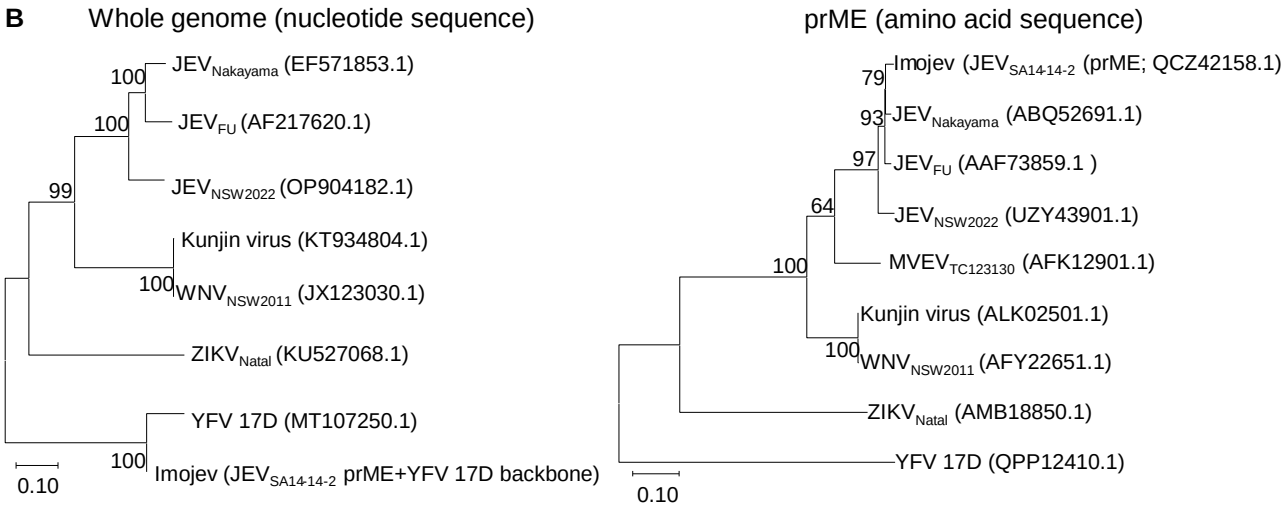

Supplementary Figure 1. (A) Summary of virus isolates used in the study. (B) Phylogenetic tree for whole genome nucleotide sequence (left) and prME amino acid sequence (right). Phylogenetic trees were constructed after nucleotide or amino acid sequence alignment using MEGA-X (Molecular Evolutionary Genetics Analysis 10, Penn State University, State College, PA, USA) and the ClustalW plugin with default parameters. The phylogenetic tree was constructed using the Maximum Likelihood method and the General Time Reversible model (nucleotide sequence) or JTT matrix-based model (amino acid sequence). Whole genome sequence is not available for $MVEV_{TC123130}$. Whole genome sequence for Imojev was constructed by combining the prME sequence from $JEV_{SA14-14-2}$ with the remainder of the genome from YFV 17D.

A

Activity

Dpi	JEV Nakayama Cg1#2	JEV Nakayama Cg1#6	JEV FU Cg2#1	MVEV Cg1#3
0	0	0	0	0
1	0	0	0	0
2	0	0	0	0
3	0	0	0	0
4	0	0	0	0
5	0	0	0	0
6	0	0	0	0
7	0	0	0	0
8	0	0	1	0
9	1	0		1
10		0		
11		1		
12				

Weight loss score

Dpi	JEV Nakayama Cg1#2	JEV Nakayama Cg1#6	JEV FU Cg2#1	MVEV Cg1#3
0	0	0	0	0
1	0	0	0	0
2	0	0	0	0
3	0	0	0	0
4	0	0	0	0
5	0	0	0	0
6	0	0	0	0
7	0	0	2	0
8	1	0	3	2
9	3	0		3
10		1		
11		3		
12				

Posture

Dpi	JEV Nakayama Cg1#2	JEV Nakayama Cg1#6	JEV FU Cg2#1	MVEV Cg1#3
0	0	0	0	0
1	0	0	0	0
2	0	0	0	0
3	0	0	0	0
4	0	0	0	0
5	0	0	0	0
6	0	0	0	0
7	0	0	0	0
8	0	0	1	0
9	1	0		1
10		0		
11		1		
12				

Fur ruffling

Dpi	JEV Nakayama Cg1#2	JEV Nakayama Cg1#6	JEV FU Cg2#1	MVEV Cg1#3
0	0	0	0	0
1	0	0	0	0
2	0	0	0	0
3	0	0	0	0
4	0	0	0	0
5	0	0	0	0
6	0	0	0	0
7	0	0	0	0
8	0	0	0	0
9	1	0		1
10		0		
11		0		
12				

B

Criteria	Level 0	Level 1	Level 2	Level 3
Joint swelling	Normal	slight to moderate swelling	Moderate/pronounce swelling and/or erythema	Joint distortion or rigidity
Injection site reaction	No reaction	Mild scaring	Moderate ulceration	Severe ulceration
Posture	Normal	Hunching noted only at rest	Severe hunching, some impairment of normal movement	Wobbling, unable to maintain upright posture
Activity	Normal	Mild to moderately decreased	Stationary unless stimulated.	Moderate paralysis, usually more than 1 limb
Fur ruffling (fever sign)	Normal	Mild to moderate ruffling	Severe ruffling	Shivering
Hind leg weakness	Normal	Mild hind limb weakness/very mild and/or occasional gait alterations	Moderate hind limb weakness and occasional dragging of hind legs	Severe hind limb weakness/repeated dragging of hind legs
Weight loss	Normal	<10 %	<15%	≥20%

Supplementary Figure 2. Disease scores for the four mice that were euthanized. (A) For the mice shown in Fig. 1E that were euthanized, the disease scores are shown. (B) The mice were monitored daily using the score card. Any animal reaching a level of 3 in any single criteria were euthanized. If an animal reaches a grade of 2 in two or more criteria the animal will be euthanized.

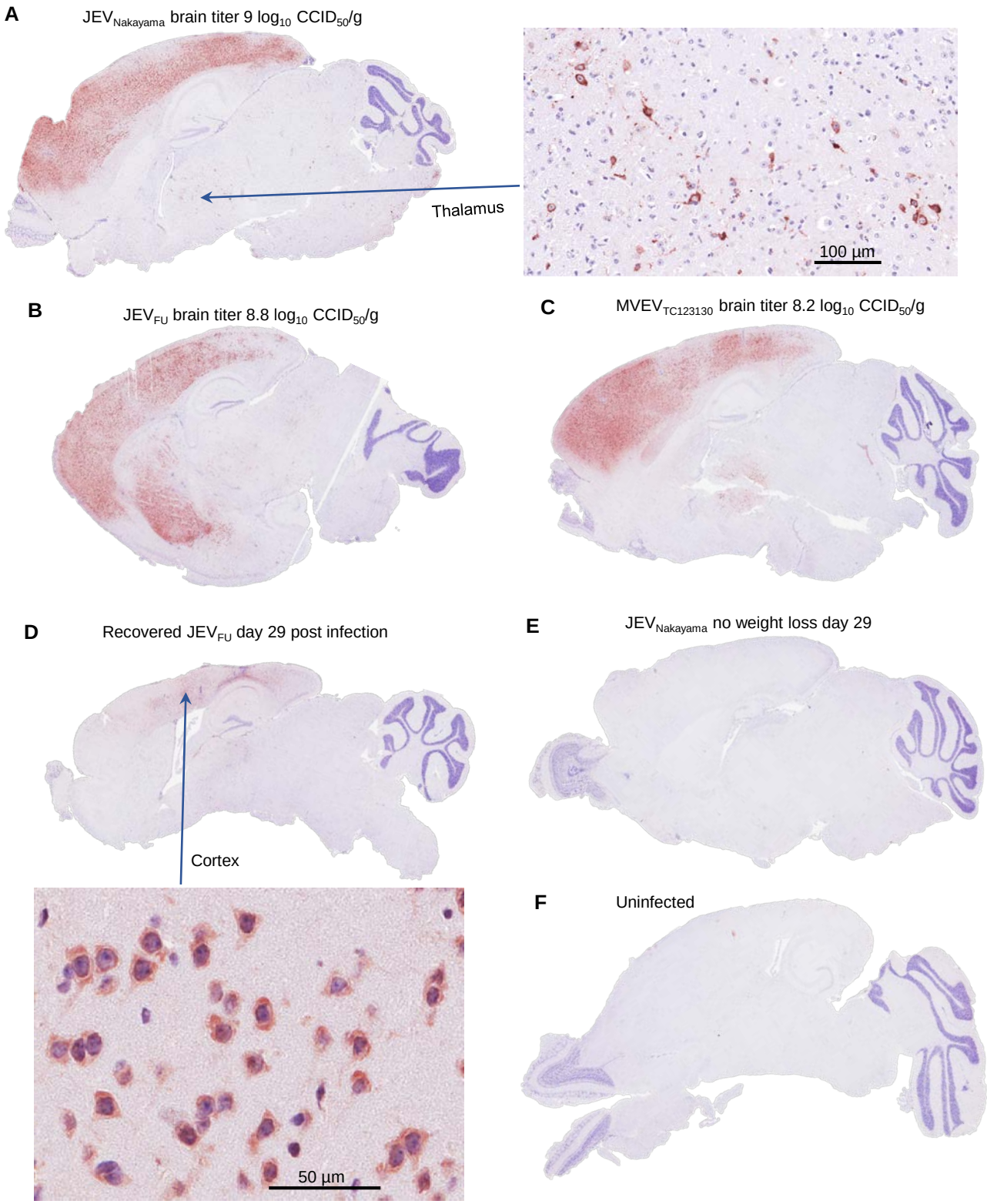

Supplementary Figure 3. Viral antigen (NS1) staining in C57BL/6J mouse brains. IHC using a pan-flavivirus NS1 monoclonal antibody (4G4). (A-C) The brains from the 3 other C57BL/6J mice that required euthanasia in Fig. 1 (the fourth is shown in Fig. 2). (D) JEV$_{FU}$ infected C57BL/6J mice that lost ~15% body weight then recovered (from Fig. 1E). (E) A representative image of a mouse brain where infection did not lead to significant weight loss. (F) Uninfected control.

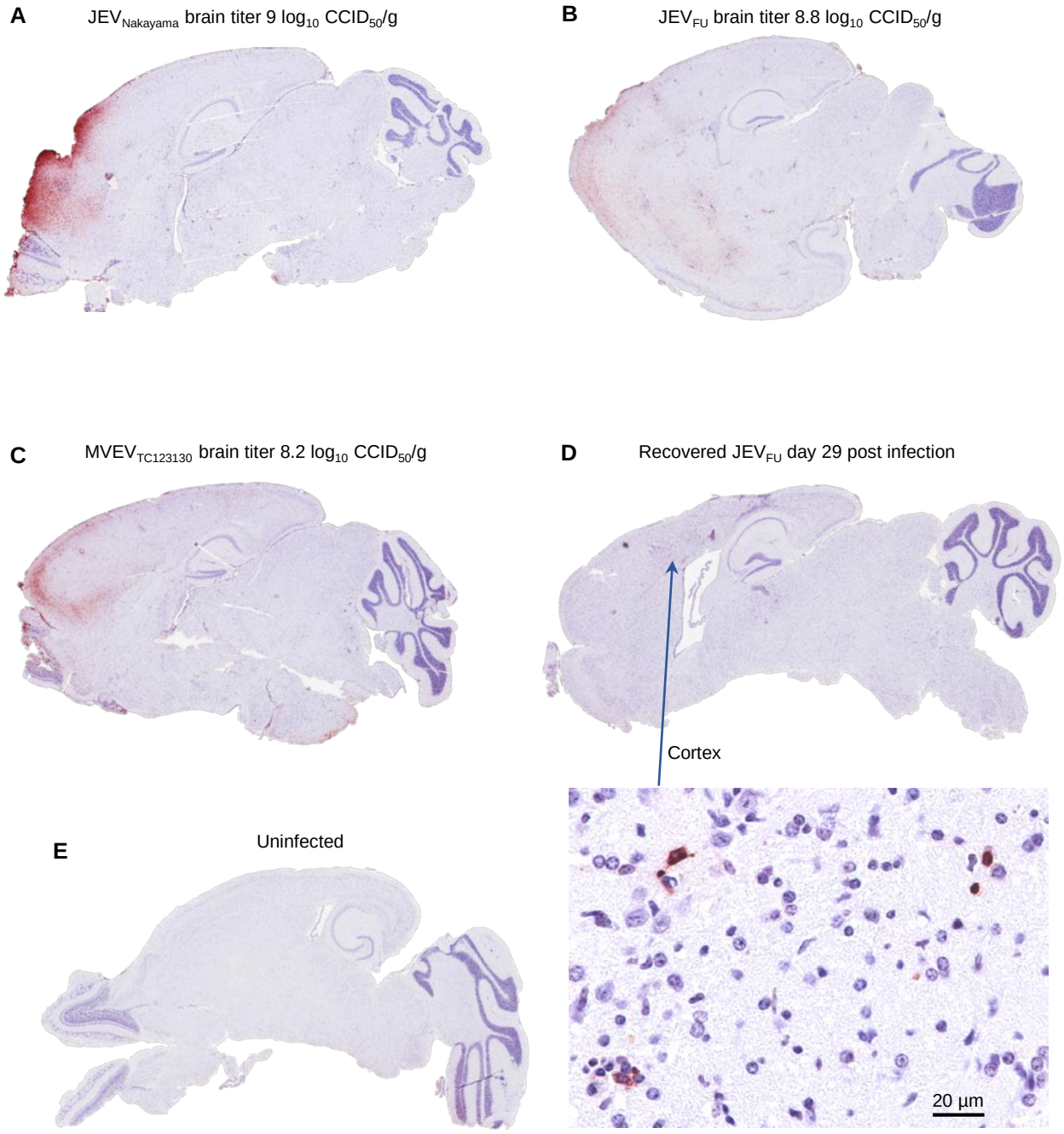

Supplementary Figure 4. ApopTag staining in C57Bl/6J mouse brains. Staining for apoptosis using Apoptag. (A-C) The brains from the 3 other C57BL/6J mice that required euthanasia in Figure 1. (D) The JEV$_{FU}$ infected C57BL/6J mice that lost ~15% body weight then recovered (see Figure 1E). (E) Uninfected control.

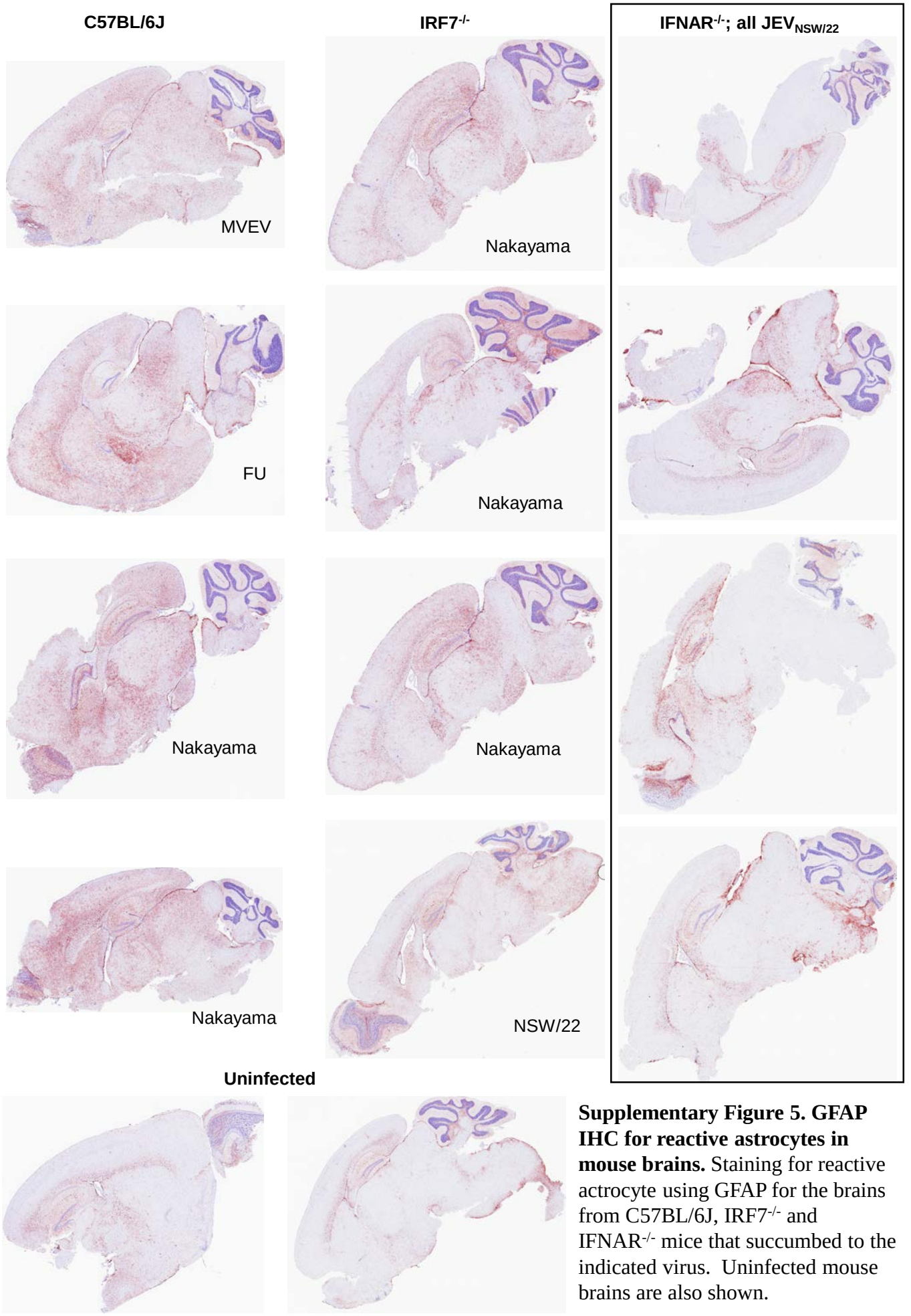

Supplementary Figure 5. GFAP IHC for reactive astrocytes in mouse brains. Staining for reactive actrocyte using GFAP for the brains from C57BL/6J, IRF7$^{-/-}$ and IFNAR$^{-/-}$ mice that succumbed to the indicated virus. Uninfected mouse brains are also shown.

A

Activity

	FU					Nakayama				NSW/22			
	Cg4#	Cg4#	Cg4#	Cg4#	Cg1#	Cg2#	Cg5#	Cg5#	Cg5#	Cg3#	Cg3#	Cg3#	Cg3#
Dpi	1	2	3	4	1	1	1	2	3	1	2	3	4
0	0	0	0	0	0	0	0	0	0	0	0	0	0
1	0	0	0	0	1	1	0	0	0	0	0	0	0
2	1	1	1	1	2	1	0	0	0	1	1	1	1
3	2	2	2	2		2	2	2	2	2	2	2	2

Weight loss score

	FU					Nakayama				NSW/22			
	Cg4#	Cg4#	Cg4#	Cg4#	Cg1#	Cg2#	Cg5#	Cg5#	Cg5#	Cg3#	Cg3#	Cg3#	Cg3#
Dpi	1	2	3	4	1	1	1	2	3	1	2	3	4
0	0	0	0	0	0	0	0	0	0	0	0	0	0
1	1	1	0	0	0	0	0	0	0	0	0	0	0
2	2	1	2	2	2	1	1	1	1	0	0	0	0
3	2	1	2	2		3	2	2	2	2	1	2	1

Posture

	FU					Nakayama				NSW/22			
	Cg4#	Cg4#	Cg4#	Cg4#	Cg1#	Cg2#	Cg5#	Cg5#	Cg5#	Cg3#	Cg3#	Cg3#	Cg3#
Dpi	1	2	3	4	1	1	1	2	3	1	2	3	4
0	0	0	0	0	0	0	0	0	0	0	0	0	0
1	0	0	0	0	0	0	0	0	0	0	0	0	0
2	1	1	1	1	1	1	1	1	0	0	0	0	0
3	2	2	2	2		2	2	2	2	2	2	2	2

Fur ruffling

	FU					Nakayama				NSW/22			
	Cg4#	Cg4#	Cg4#	Cg4#	Cg1#	Cg2#	Cg5#	Cg5#	Cg5#	Cg3#	Cg3#	Cg3#	Cg3#
Dpi	1	2	3	4	1	1	1	2	3	1	2	3	4
0	0	0	0	0	0	0	0	0	0	0	0	0	0
1	0	0	0	0	0	0	0	0	0	0	0	0	0
2	1	1	1	1	0	0	0	0	0	0	0	0	0
3	1	1	1	1		0	1	1	1	0	0	0	0

B

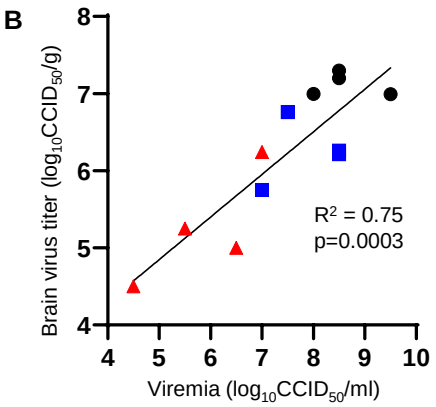

C

$JEV_{NSW/22}$ brain $IFNAR^{-/-}$ mouse, 3 dpi, titer 6.6 log_{10} $CCID_{50}$/g

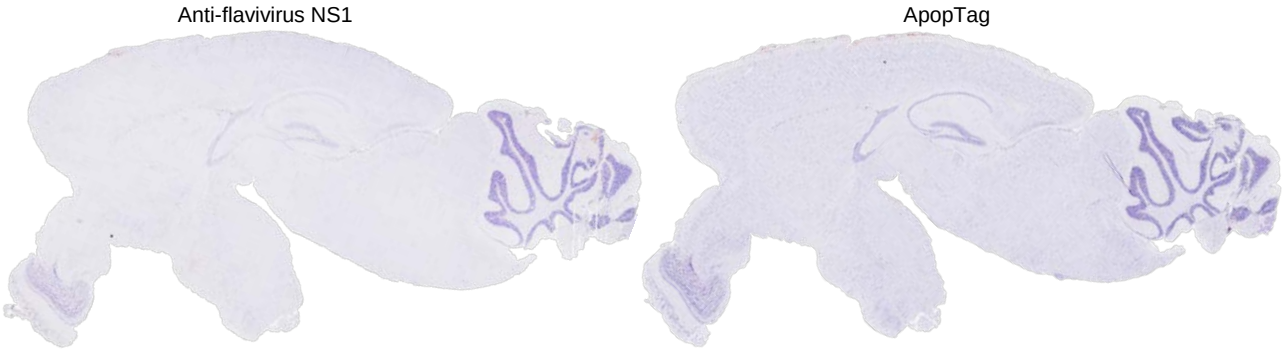

Supplementary Figure 6. JEV infection of $IFNAR^{-/-}$ mice. (A) Disease scores as per Supplementary Figure 2B for mice shown in Figure 3. (B) Pearson correlation between brain titer (y-axis) from Figure 3E and viremia (x-axis) from Figure 3A. (B) IHC for flavivirus NS1 (left) or ApopTag (right) showing no detectable staining of brain cells. Images are representative of all $IFNAR^{-/-}$ brains and JEV isolates.

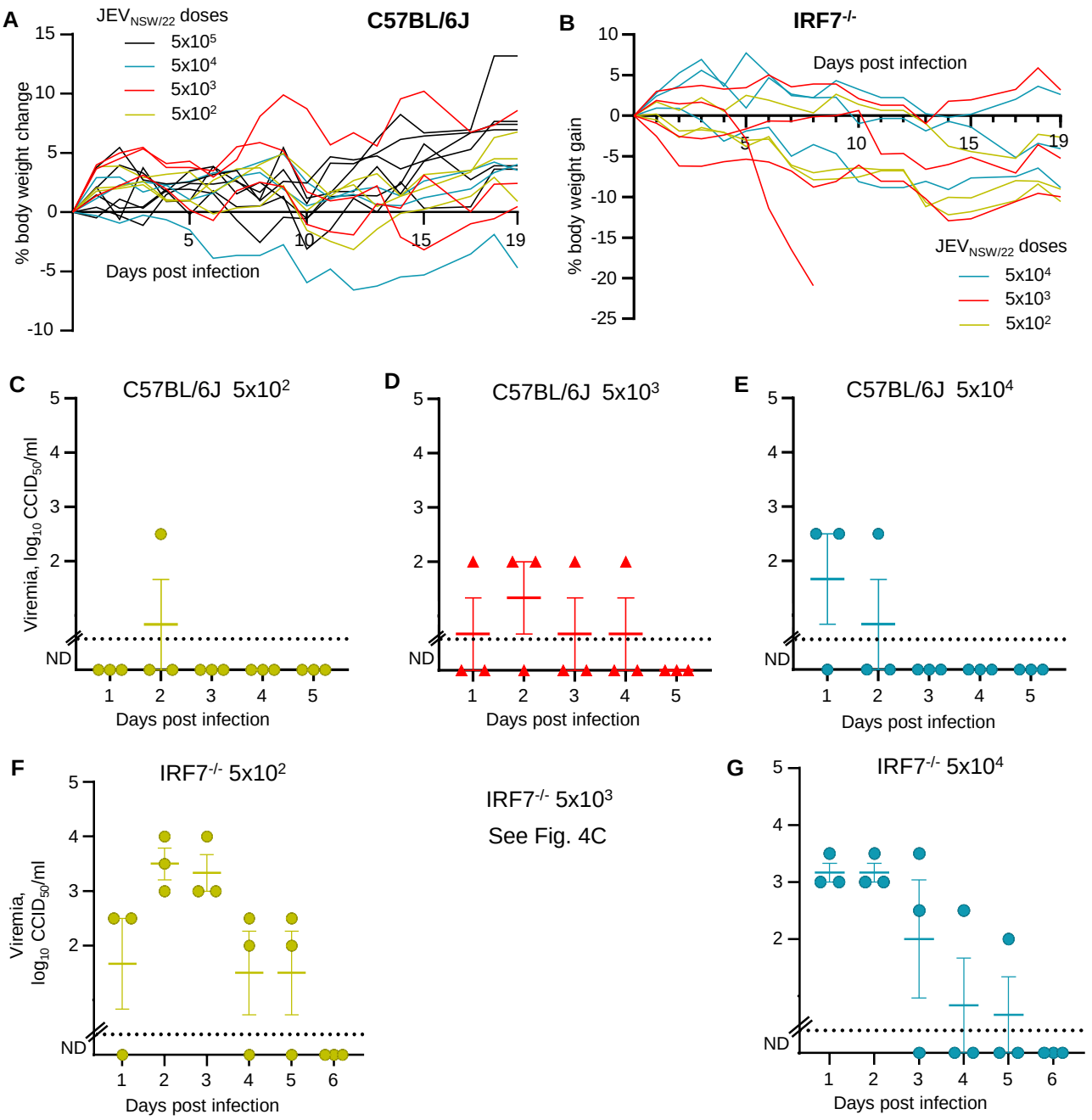

Supplementary Figure 7. $JEV_{NSW/22}$ dose range in C57BL/6J and $IRF7^{-/-}$ mice. Adult female C57BL/6J mice (15 weeks of age) or $IRF7^{-/-}$ mice (15-48 weeks of age) were infected s.c. with $JEV_{NSW/22}$ at the indicated $CCID_{50}$ doses of $JEV_{NSW/22}$. (A) Percent body weight change of individual C57BL/6J mice compared to each mouse's weight 0 dpi. (B) As for A but using $IRF7^{-/-}$ mice. The data for $5x10^3$ is the same as Figure 4E, showing individual mice. (C-E) Viremia for C57BL/6J mice infected with the indicated doses, determined by $CCID_{50}$ assays with a limit of detection of ~2 $log_{10}CCID_{50}$/ml. Horizontal lines indicate mean at each time point, and error bars represent SE. (F-G) As for C-E but for $IRF7^{-/-}$ mice.

Activity

		Nakayama					NSW/22	FU							
Dpi	Cg1#1	Cg1#2	Cg1#3	Cg5#1	Cg1#1	Cg3#1	Cg2#1	Cg19#1	Cg19#2	Cg19#3	Cg19#4	Cg11#1	Cg12#1	Cg14#1	Cg14#2
0	0	0	0	0	0	0	0	0	0	0	0	0	0	0	0
1	0	0	0	0	0	0	0	0	0	0	0	0	0	0	0
2	0	0	0	0	0	0	0	0	0	0	0	0	0	0	0
3	0	0	0	0	0	0	0	0	0	0	0	0	0	0	0
4	0	0	0	0	0	0	0	0	0	0	0	0	0	0	0
5	0	0	0	0	0	0	0	0	0	0	0	0	0	0	0
6	0	0	0	0	0	0	0	0	3	0	2	1	0	0	0
7	0	1	0	1	0	0	0	2		2		1	0	2	0
8	0		2	1	0	0	1					2	0		2
9	0				2	0							1		
10	0												1		
11	1														
12	2														

Posture

		Nakayama					NSW/22	FU							
Dpi	Cg1#1	Cg1#2	Cg1#3	Cg5#1	Cg1#1	Cg3#1	Cg2#1	Cg19#1	Cg19#2	Cg19#3	Cg19#4	Cg11#1	Cg12#1	Cg14#1	Cg14#2
0	0	0	0	0	0	0	0	0	0	0	0	0	0	0	0
1	0	0	0	0	0	0	0	0	0	0	0	0	0	0	0
2	0	0	0	0	0	0	0	0	0	0	0	0	0	0	0
3	0	0	0	0	0	0	0	0	0	0	0	0	0	0	0
4	0	0	0	0	0	0	0	0	0	0	0	0	0	0	0
5	0	0	0	0	0	0	0	0	0	0	0	0	0	0	0
6	0	0	0	0	0	0	0	0	2	0	2	1	0	0	0
7	0	2	0	1	0	0	0	1		1		1	0	1	0
8	0		2	1	0	0	1					2	0		2
9	0				2	1							1		
10	0												2		
11	1														
12	2														

Weight loss score

		Nakayama					NSW/22	FU							
Dpi	Cg1#1	Cg1#2	Cg1#3	Cg5#1	Cg1#1	Cg3#1	Cg2#1	Cg19#1	Cg19#2	Cg19#3	Cg19#4	Cg11#1	Cg12#1	Cg14#1	Cg14#2
0	0	0	0	0	0	0	0	0	0	0	0	0	0	0	0
1	0	0	0	0	0	0	0	0	0	0	0	0	0	0	0
2	0	0	0	0	0	0	0	0	0	0	0	0	0	0	0
3	0	0	0	0	0	0	0	0	0	0	0	0	0	0	0
4	0	0	0	0	0	0	0	0	0	0	0	0	0	0	0
5	0	0	0	0	0	0	0	0	0	0	0	0	0	0	0
6	0	0	0	1	0	0	0	0	1	0	1	2	0	0	0
7	0	2	0	2	0	1	0	3		2		2	1	2	0
8	0		1	3	1	2	3					3	1		3
9	0				3	3							2		
10	0												3		
11	2														
12	3														

Fur ruffling

		Nakayama					NSW/22	FU							
Dpi	Cg1#1	Cg1#2	Cg1#3	Cg5#1	Cg1#1	Cg3#1	Cg2#1	Cg19#1	Cg19#2	Cg19#3	Cg19#4	Cg11#1	Cg12#1	Cg14#1	Cg14#2
0	0	0	0	0	0	0	0	0	0	0	0	0	0	0	0
1	0	0	0	0	0	0	0	0	0	0	0	0	0	0	0
2	0	0	0	0	0	0	0	0	0	0	0	0	0	0	0
3	0	0	0	0	0	0	0	0	0	0	0	0	0	0	0
4	0	0	0	0	0	0	0	0	0	0	0	0	0	0	0
5	0	0	0	0	0	0	0	0	0	0	0	0	0	0	0
6	0	0	0	0	0	0	0	0	0	0	1	1	0	0	0
7	0	2	0	1	0	0	0	0		0		1	0	0	0
8	0		1	1	1	0	1					1	0		1
9	0				3	1							1		
10	0												2		
11	0														
12	0														

Supplementary Figure 8. Disease scores for IRF7-/- mice that were euthanized. Mice described in Figure 4E, F. Scoring system shown in Supplementary Figure 2B.

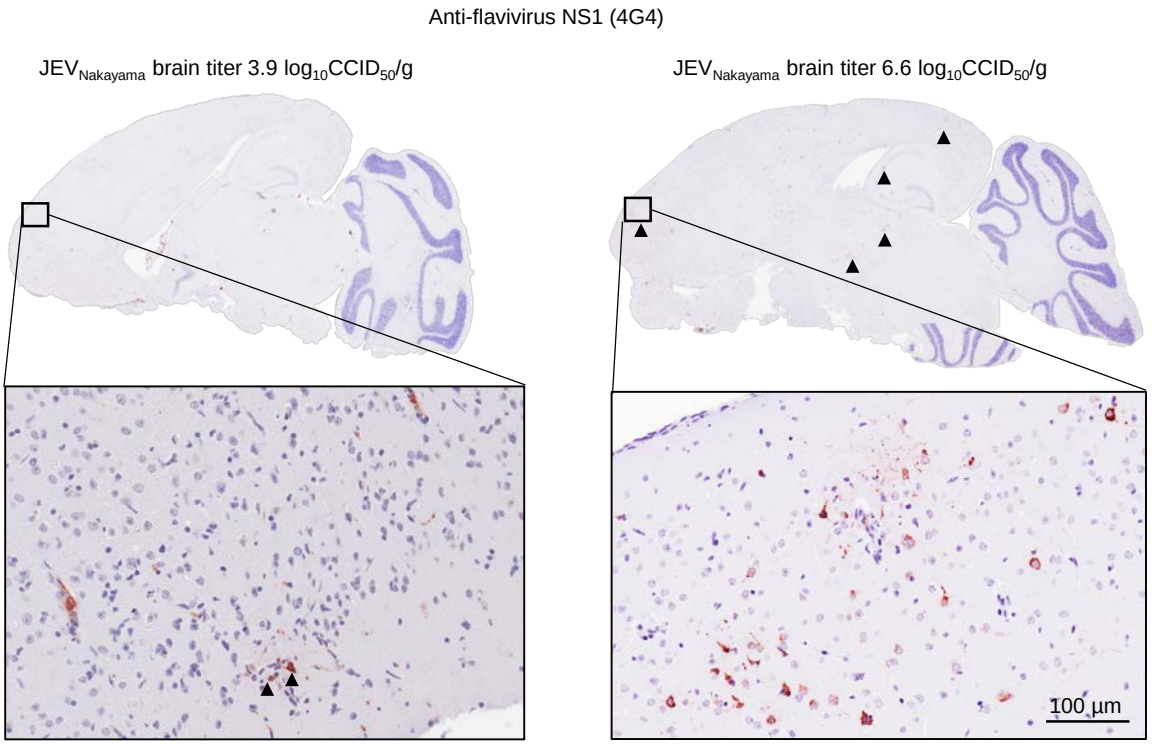

Supplementary Figure 9. Viral antigen staining in IRF7$^{-/-}$ mouse brains. IHC using a pan-flavivirus NS1 monoclonal antibody (4G4) for the brains from the 2 other IRF7$^{-/-}$ mice that required euthanasia (Figure 3). Low levels of staining of neurons were found in the JEV$_{Nakayama}$ infected mice that had a low virus titer in the brain (3.9 log$_{10}$CCID$_{50}$/g) (left). Black arrowheads show small patches of staining in the cortex, hippocampus and thalamus (right).

Acute (euthanized due to weight loss/disease scores)

Mouse	C57BL/6J			IRF7-/-			IFNAR-/-		
JEV isolate	NSW	Nakayama	FU	NSW	Nakayama	FU	NSW	Nakayama	FU
Euthanasia		9-11 dpi	8 dpi	8 dpi	7-12 dpi	6-10 dpi	3 dpi	3 dpi	3 dpi
Neuronal degeneration /vacuolation	**N/A**	**2/2**	**1/1**	**0/1**	**2/6**	**5/8**	**0/4**	**0/3**	**0/4**
Perivascular cuffing	**N/A**	**2/2**	**1/1**	**1/1**	**6/6**	**8/8**	**0/4**	**0/3**	**0/4**
Hemorrhage	**N/A**	**2/2**	**1/1**	**0/1**	**5/6**	**5/8**	**3/4**	**2/3**	**2/4**
Leukocyte infiltrates	**N/A**	**2/2**	**1/1**	**1/1**	**1/6**	**3/8**	**0/4**	**0/3**	**0/4**
Microgliosis	**N/A**	**2/2**	**1/1**	**0/1**	**3/6**	**6/8**	**0/4**	**0/3**	**0/4**
Meningitis	**N/A**	**2/2**	**1/1**	**1/1**	**5/6**	**6/8**	**0/4**	**0/3**	**0/3**

Chronic (euthanized after recovery from acute phase)

Mouse	C57BL/6J			IRF7-/-		
JEV isolate	NSW	Nakayama	FU	NSW	Nakayama	FU
Euthanasia	32 dpi	32 dpi	32 dpi	19 dpi	19 dpi	
Neuronal degeneration /vacuolation	**0/6**	**0/4**	**0/5**	**0/3**	**0/1**	**N/A**
Perivascular cuffing	**0/6**	**0/4**	**1/5**	**0/3**	**1/1**	**N/A**
Hemorrhage	**1/6**	**2/4**	**1/5**	**1/3**	**1/1**	**N/A**
Leukocyte infiltrates	**0/6**	**0/4**	**1/5**	**0/3**	**0/1**	**N/A**
Microgliosis	**0/6**	**0/4**	**2/5**	**1/3**	**1/1**	**N/A**
Meningitis	**0/6**	**0/4**	**0/5**	**0/3**	**1/1**	**N/A**

Supplementary Figure 10. Lesion presence in H&E brain sections. For lesions described in Figure 5. H&E scoring of 0 indicates no overt presence of these lesions. N/A – not available; no NSW-infected C57BL/6J mice died of acute infection, and all FU infected IRF7$^{-/-}$ mice died of acute disease.

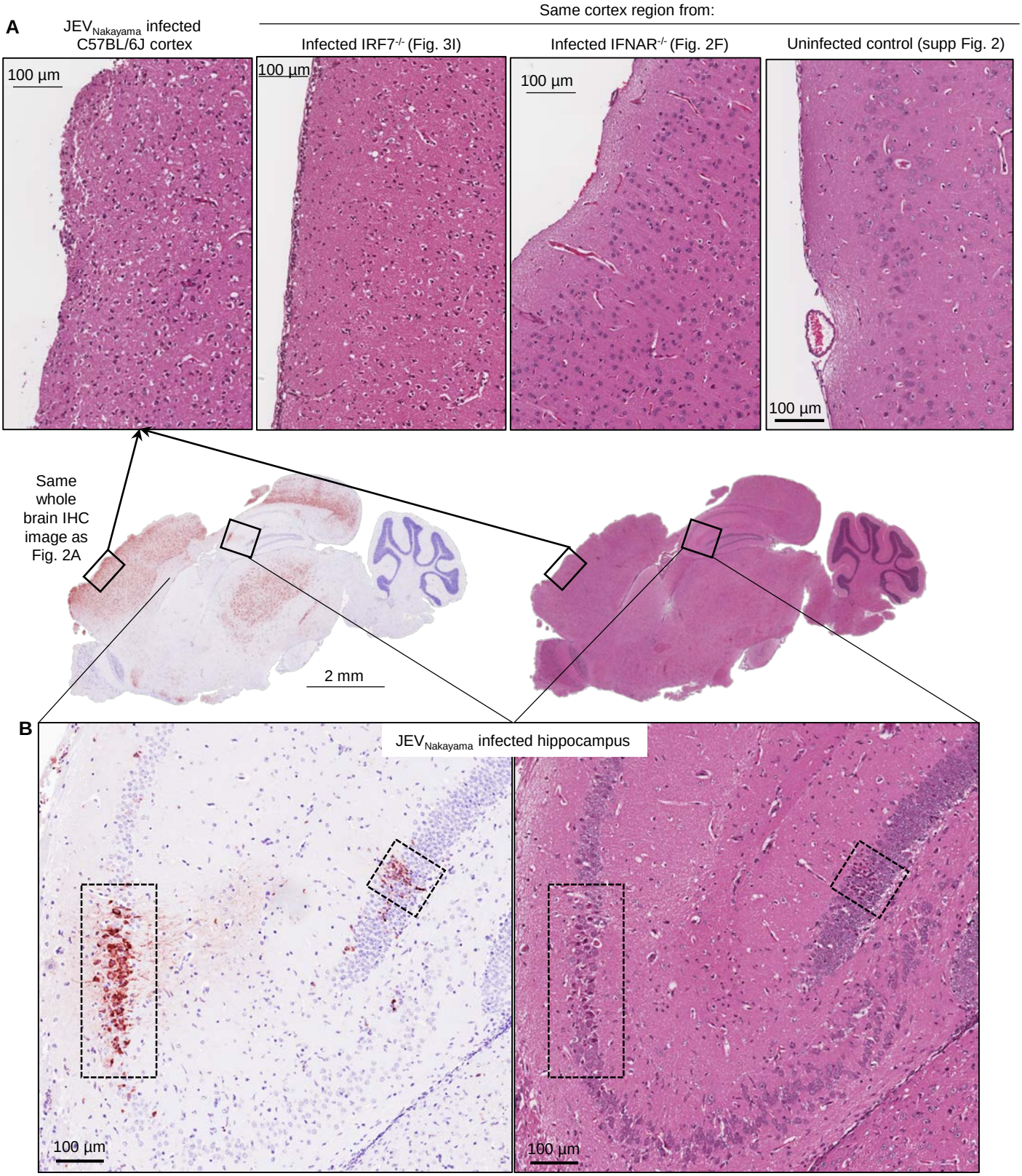

Supplementary Figure 11. Histopathological lesions overlapped with areas of virus infection. (A) Cortex regions from JEV infected C57BL/6J, IRF7$^{-/-}$, IFNAR$^{-/-}$ mice or uninfected mice. The cortex regions from JEV infected mice were heavily infected, with most neurons stained positive for viral antigen. H&E detectable signs of neuron degeneration/vacuolation were concentrated in regions with high staining for viral antigen. (B) Viral antigen staining (left) in hippocampus overlapped with histological signs of neuron degeneration/vacuolation (right) (see Figure 5).

A IRF7$^{-/-}$ and C57BL/6J mice (n=18) that were euthanized due to ethically defined disease end points

	Neuron degeneration/ vacuolation	Perivascular cuffing	Hemorrhage	Leukocyte infiltrates	Microgliosis
Cerebral cortex	**9/18**	**14/18**	**5/18**	**5/18**	**3/18**
Hypothalamus	**0/18**	**4/18**	**3/18**	**2/18**	**4/18**
Thalamus	**0/18**	**11/18**	**2/18**	**2/18**	**7/18**
Hippocampus	**0/18**	**5/18**	**0/18**	**0/18**	**4/18**
Caudate putamen	**1/18**	**9/18**	**1/18**	**2/18**	**3/18**
Basal forebrain	**0/18**	**6/18**	**2/18**	**0/18**	**0/18**
Midbrain	**0/18**	**7/18**	**1/18**	**0/18**	**3/18**
Pons	**0/18**	**4/18**	**3/18**	**1/18**	**1/18**
Medulla	**0/18**	**3/18**	**0/18**	**0/18**	**0/18**
Cerebellum	**0/18**	**3/18**	**1/18**	**0/18**	**0/18**

B IRF7$^{-/-}$ and C57BL/6J mice (n=19) that survived infection (taken on day 19 and day 32, respectively)

	Neuron degeneration/ vacuolation	Perivascular cuffing	Hemorrhage	Leukocyte infiltrates	Microgliosis
Cerebral cortex	**0/19**	**2/19**	**2/19**	**1/19**	**4/19**
Hypothalamus	**0/19**	**0/19**	**2/19**	**0/19**	**0/19**
Thalamus	**0/19**	**0/19**	**0/19**	**0/19**	**2/19**
Hippocampus	**0/19**	**0/19**	**0/19**	**0/19**	**0/19**
Caudate putamen	**0/19**	**0/19**	**0/19**	**0/19**	**2/19**
Basal forebrain	**0/19**	**1/19**	**4/19**	**0/19**	**0/19**
Midbrain	**0/19**	**0/19**	**0/19**	**0/19**	**0/19**
Pons	**0/19**	**0/19**	**1/19**	**0/19**	**0/19**
Medulla	**0/19**	**0/19**	**0/19**	**0/19**	**0/19**
Cerebellum	**0/19**	**1/19**	**2/19**	**0/19**	**0/19**
Anterior olfactory nucleus	**0/19**	**0/19**	**1/19**	**0/19**	**0/19**
Ventral striatum	**0/19**	**0/19**	**2/19**	**0/19**	**0/19**

Supplementary Figure 12. Histopathological lesions in specific brain regions for C57BL/6J and IRF7$^{-/-}$. Scoring only reflects presence or absence of lesions, and does not indicate severity of lesions. (A) Acute (B) Chronic.

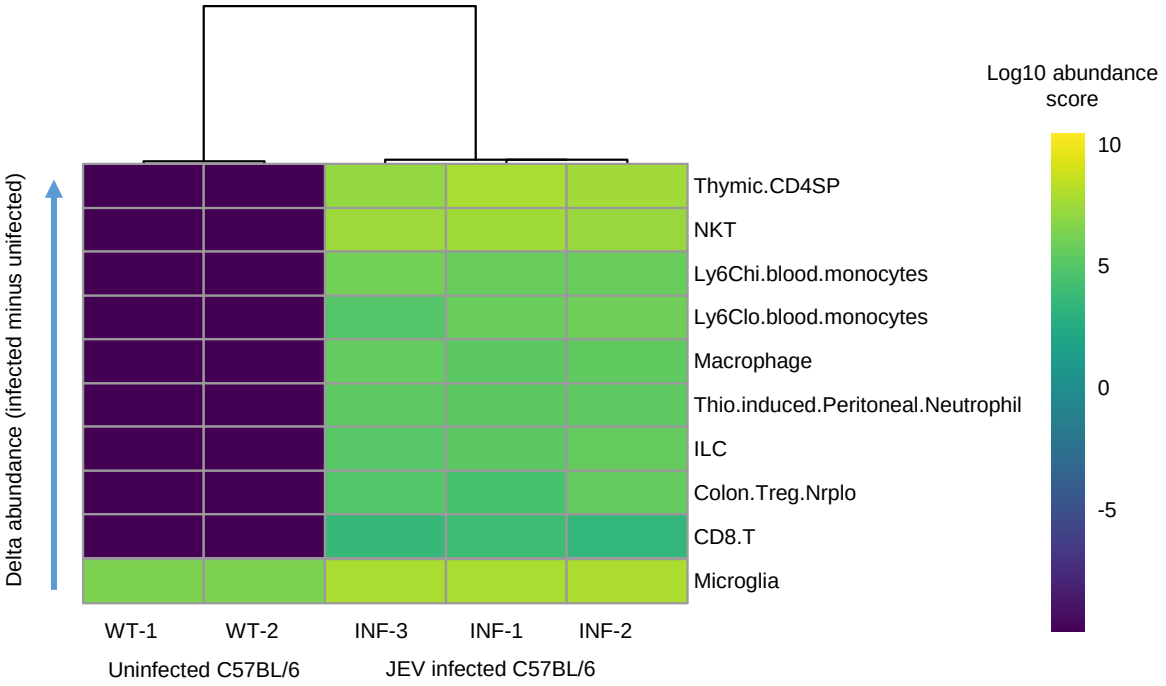

Supplementary Figure 13. RNA-Seq read counts from brains of C57BL/6 JEV-infected and mock-infected mice obtained from the Gene Expression Omnibus (GEO accession: GSE154002) were normalised for sequencing depth and composition using DESeq2. An estimation of cell type abundances was performed on normalised read counts with the SpatialDecon package in R, using an adult mouse immune cell gene expression reference (Yoshida *et al.* 2019. Cell 176; 897-912.e20). Log_{10} abundance scores are shown for cell types that were significantly different between infected and mock-infected groups (t-test, p-value < 0.05), with cell types ordered from largest to smallest difference in mean abundance score between groups.

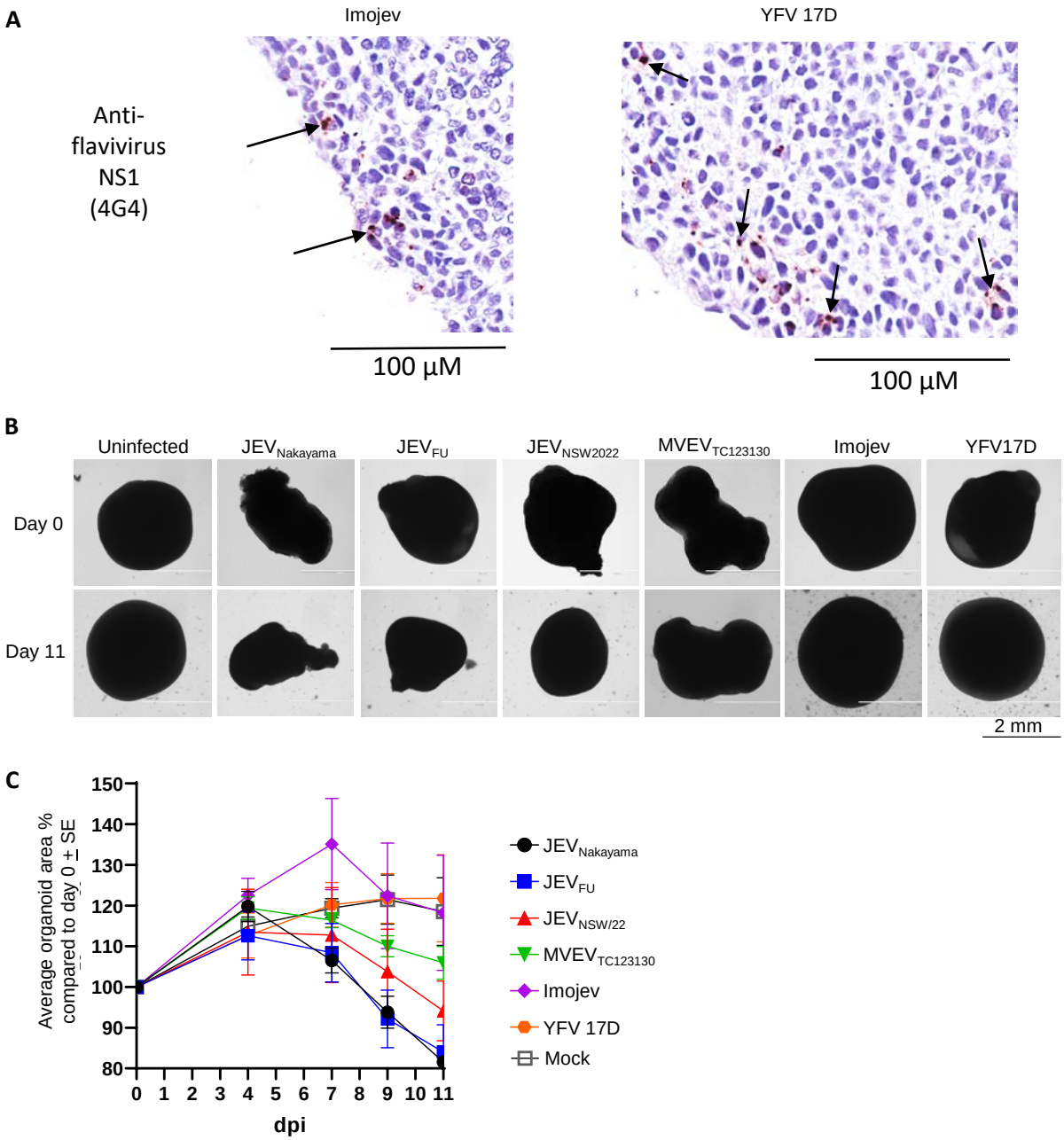

Supplementary Fig. 14. Human cortical brain organoids measurements and magnified virus staining. (A) Occasional cells staining positive for IHC for viral antigen in hBOs infected with Imojev or YFV 17D. (B) Light microscopy images of hBOs infected with $JEV_{Nakayama}$, JEV_{FU}, $JEV_{NSW2022}$, $MVEV_{TC123130}$, Imojev or YFV 17D at day 0 and day 11 post infection compared to uninfected hBOs. Scale bar is consistent across all images. (C) Change in hBO area on day 4, 7, 9 and 11 compared to day 0. n=8 for uninfected and $MVEV_{TC123130}$, n=4 for all others.

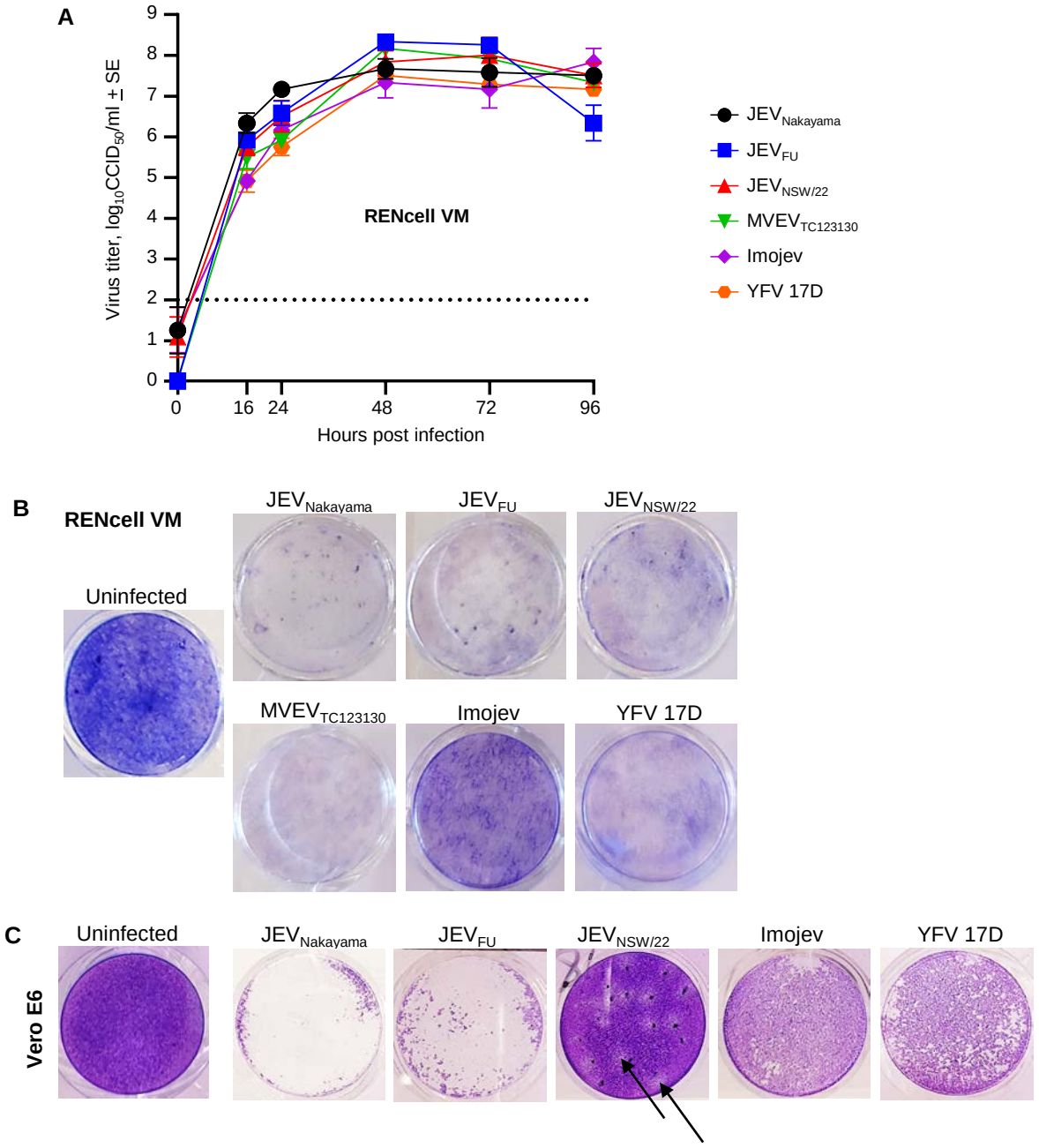

Supplementary Figure 15. Replication and CPE in RENcell VM neural progenitor and Vero E6 cell lines. (A) Viral growth kinetics in RENcell VM determined by $CCID_{50}$ assays of culture supernatant at the indicated times post infection. Data is the mean of 6 replicates per virus isolate across 2 independent experiments; (limit of detection is 2 $log_{10}CCID_{50}$/ml). (B) Images of crystal violet stained RENcell VM at 6 dpi (representative of n=3 per group). Less blue/violet stained cells indicates more viral CPE. (C) Vero cells were seeded at $2.5x10^5$ cells per well in 24 well plates overnight at 37°C. Cells were infected at MOI=0.05 for 1 hr at 37°C before overlay media (0.375% w/v high viscosity carboxymethyl cellulose [CMC, Sigma-Aldrich]/RPMI 1640 substituted with 2% FCS) was added to each well. Plates were incubated for 5 days before the media was removed and monolayers were fixed and stained with 0.1% w/v crystal violet (Sigma-Aldrich) in formaldehyde (1% v/v) and methanol (1% v/v). Plates were washed in tap water and dried before images were taken. Images shown are representative of n=4 per group. CPE is less pronounced in $JEV_{NEW/22}$ infected cells, with plaques (arrows), rather than fulminant CPE, apparent at 5 dpi.

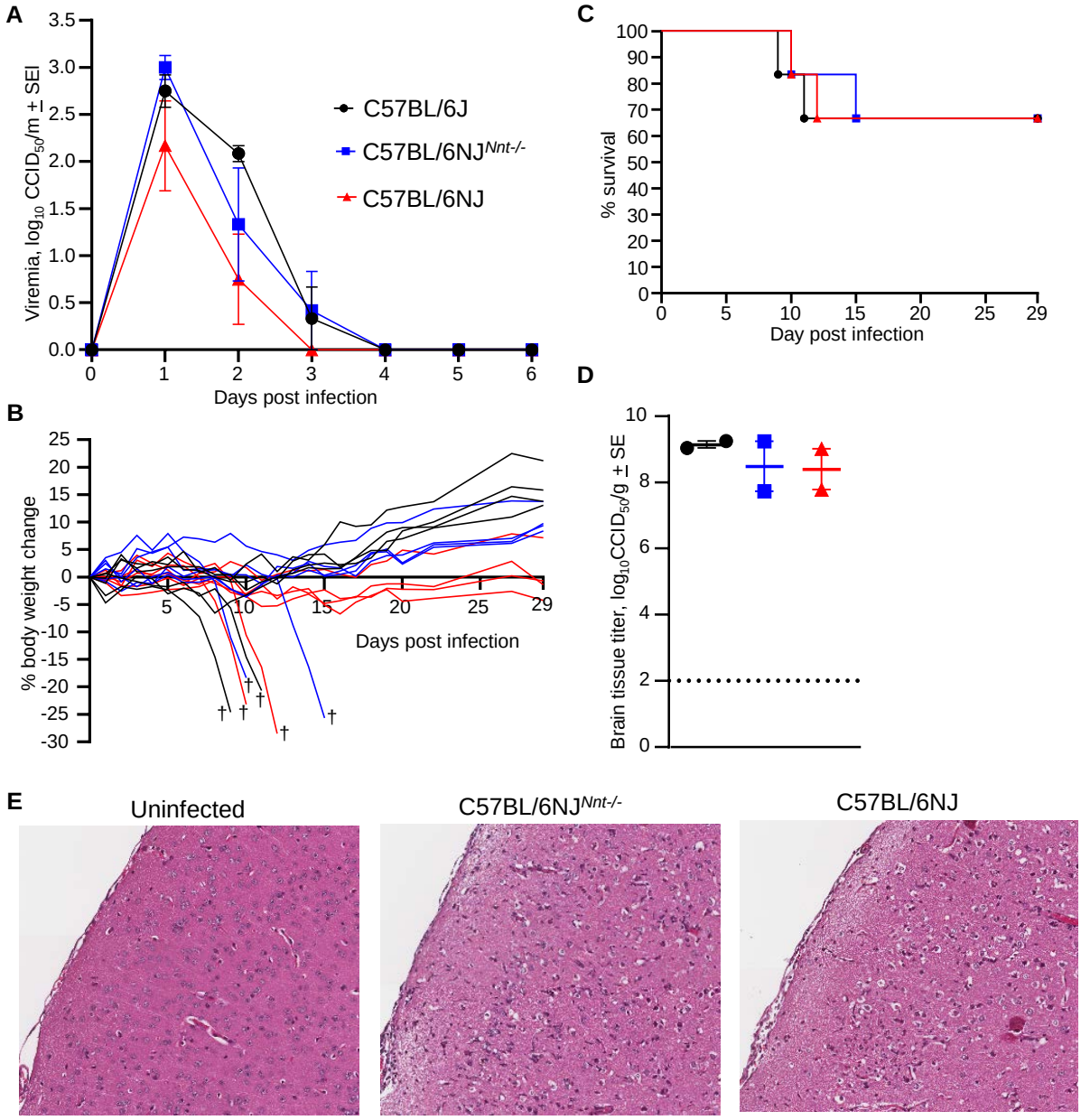

Supplementary Fig. 16. Neither mouse background nor *Nnt* significantly affected JEV neuropathogenesis. Female C57BL/6J (10-16 weeks old) (black circles), C57BL/6NJ$^{Nnt-/-}$ (blue squares), and C57BL/6NJ (red triangles) mice were infected s.c. with $5x10^5$ $CCID_{50}$ $JEV_{Nakayama}$. (A) Average viremia as determined by $CCID_{50}$ assays; limit of detection for individual mice is 2 $log_{10}CCID_{50}$/ml. (B) Percent body weight change of individual mice compared to their weight 0 dpi. Six mice lost ≥20% body weight and required euthanasia (†). (C) Kaplan Myer plot showing percent survival (n=6 for each mouse strain). (D) Viral tissue titers in brains of the six euthanized mice (n=2 from each mouse strain). Tissue titers determined by $CCID_{50}$ assays (limit of detection ~2 $log_{10}CCID_{50}$/g). (E) Representative images of H&E stained sections of brains from mice that required euthanasia. No overt differences were identified between C57BL/6J, C57BL/6NJ$^{Nnt-/-}$, or C57BL/6NJ mice.